THE DEVELOPMENT OF A FUNCTIONAL MAGNETOMETER FOR MEASUREMENT OF REMANENT MAGNETIZATION

Thesis for the Degree of M. S.
MICHIGAN STATE UNIVERSITY
THOMAS WILLIAM MacCLURE
1970

ABSTRACT

THE DEVELOPMENT OF A FUNCTIONAL MAGNETOMETER FOR MEASUREMENT OF REMANENT MAGNETIZATION

By

Thomas William MacClure

A functional spinner magnetometer for the measurement of the remanent magnetization of igneous rocks was constructed. This instrument is a modification of the original design by Doell and Cox of the U.S. Geological Survey. These design modifications were made to enhance the versatility and efficiency of the magnetometer.

Cross checks of rock sample measurements made by other laboratories showed excellent correlation of measurement capabilities and results.

A suite of rock samples from the Melrose stock, located in eastern Nevada was investigated to demonstrate an application of the instrument. No correlation was found to exist between the intensity of the natural remanent magnetization and the magnetite content of prophyritic quartz monzonite or the distance of samples from the contact of the igneous intrusive.

THE DEVELOPMENT OF A FUNCTIONAL MAGNETOMETER FOR MEASUREMENT OF REMANENT MAGNETIZATION

By

Thomas William MacClure

A THESIS

Submitted to
Michigan State University
in partial fulfillment of the requirements
for the degree of

MASTER OF SCIENCE

Department of Geology

1970

ACKNOWLEDGMENTS

The author wishes to express his sincere appreciation to:

Dr. William Hinze, of the Geology Department, Michigan State University, for his patient guidance, constant understanding, constructive criticism and advice throughout this study.

Dr. LeRoy Scharon, of the Department of Earth Sciences, Washington University, St. Louis, Missouri, for the valuable assistance in providing constructional details on the instrument. Dr. Scharon also permitted the author to take photographs of the Washington University spinner magnetometer and donated a secondary standard sample.

Mr. I-chi Hsu, graduate student, Washington University, for advice and for providing comparison measurements made on several samples.

Dr. Richard Doell, of the Branch of Regional Geophysics, U.S. Geological Survey, Menlo Park, California, for advice and for the loan of three measured samples.

Mr. Major Lillard, of the Branch of Regional Geophysics, U.S. Geological Survey, for assistance regarding constructional details of the magnetometer.

Mr. Edward Mankinen, of the Branch of Regional Geophysics, U.S. Geological Survey, for advice and for the measurement and calculation of results of several samples on two different occasions.

Associate Professor Ralph Vanderslice, of the Engineering Technology Department, Lansing Community College, Lansing, Michigan, for the machining of several of the principal parts of the spinner magnetometer.

Mr. Dewey Sanderson, graduate student, Geology Department, Michigan State University, for collecting the samples studied and assistance with the measurements and computer programs used in analyzing the operation of the spinner magnetometer.

Mr. Wayne Wilson, Electronics Technician, Geology Department, Michigan State University, for machining of several plastic components and winding of the coils used in the magnetometer.

TABLE OF CONTENTS

LIST OF TABLES

LIST OF FIGURES

CHAPTER I

INTRODUCTION

Magnetic characteristics are demonstrated by all rocks to varying degrees. Basically, these characteristics are of two types; induced and permanent magnetization. Induced magnetism, because it originates and depends upon a supporting magnetic field, is of a temporary nature. In contrast, permanent, or natural remanent magnetism (NRM), remains in the absence of a magnetic field. Paleomagnetism is a branch of the science of geophysics which is concerned with the study of the NRM of rocks, which was acquired at the time of their formation, or as a result of subsequent modification due to environmental change.

During the past three decades paleomagnetism has been a rapidly expanding area of geophysical study because of its use in solving a wide variety of geological problems. Furthermore, paleomagnetic studies have shown that NRM is an important contributor to the total magnetization of many rocks. Therefore, knowledge of the permanent magnetization of rocks plays an important role in the geological interpretation of geomagnetic anomalies.

Seven processes have been identified by which rocks may acquire NRM. Each of these has been studied extensively by theoretical and experimental methods. The details of these processes have been described by Nagata (1961). The type of NRM acquired by a rock is dependent upon the formation process and subsequent geological and magnetic history of the rock. Each of these processes are briefly described below.

Anhysteretic remanent magnetization (ARM) is developed by the concurrent effect of an alternating magnetic field of smoothly diminishing aplitude superimposed on a constant magnetic field. Under natural conditions ARM is produced by lightning in the presence of the earth's geomagnetic field.

Chemical remanent magnetization (CRM) is developed through crystalization or chemical change of ferrimagnetic minerals, within a magnetic field at low (even below the Curie point) temperatures. It may produce the initial NRM or modify existing NRM in metamorphic, weathered, or altered rocks.

Depositional remanent magnetization (DRM) is developed by the alignment of the ferromagnetic mineral particles during the formation of sedimentary rocks by deposition within the influence of a magnetic field. It normally produces a less inclined dip than that of the ambient value of the geomagnetic field due to compaction of the sediments.

Isothermal remanent magnetization (IRM) is the normal type of magnetization associated with the hysteresis curve. It is acquired by ferrimagnetic grains when placed in a magnetic field greater than the smallest coercive force of any domain of the grains.

Viscous remanent magnetization (VRM) is displayed by rocks exposed to the geomagnetic field for an extended (geologic) length of time.

Piezo remanent magnetization (PRM) is developed by magnetostriction through the concurrent effect of pressure and a magnetic field.

Thermo-remanent magnetization (TRM) is developed in rocks which have cooled after being exposed to elevated temperatures above the Curie point within a magnetic field. This is the source of NRM in most igneous rocks.

Many field and laboratory techniques have been developed for measuring the NRM of rocks. One of the most successful methods of laboratory measurements is the spinner type magnetometer. Doell and Cox (1965) have described an instrument of this type for measuring the NRM of igneous rocks. The purpose of this thesis was to construct this instrument incorporating several design modifications to improve its versatility and operational efficiency calibrate the instrument, and determine its precision. In addition the NRM of a suite of oriented core samples collected from the Melrose stock in eastern Nevada was measured to

demonstrate the operation and application of the spinner type magnetometer.

The magnetometer is utilized to determine the declination, inclination, and intensity of the NRM of oriented rock samples over an intensity range of 1 to 1×10^{-6} emu/cm^3 with a phase error of less than one degree and an intensity error of less than 2 per cent. This information may be used for geological and geophysical studies of polar wandering, continental drift, stratigraphic correlation, structural and petrologic problems, and the interpretation of geomagnetic anomalies.

CHAPTER II

MEASUREMENT METHODS

Several different methods have been devised to measure the remanent magnetization of rocks. Among these are the alternating current (spinner) magnetometer, astatic magnetometer, ballistic galvanometer, and magnetic balance methods. Each method is considered briefly below.

The alternating current (spinner) magnetometer operates on the principle of an alternating current generator in which the magnetic field about a rotating rock sample induces a voltage in a stationary pick-up coil assembly. This voltage is then amplified and compared to a reference signal of known phase and amplitude for measurement of the phase and intensity of the magnetic component of the rock sample perpendicular to its axis of rotation. The advantages of the spinner magnetometer are the high degree of measurement accuracy, comparative freedom from drift over considerable periods of time (several years), ease with which the 12 measurement (plus and minus X, Y and Z axis intensity and phase) technique can be executed. It lends itself well to paleomagnetic studies where a sensitivity of a high order is unnecessary, but a high order of

accuracy is important, the effects of susceptibility anisotropy can be maintained negligible and sample inhomogeneity are also negligible. Disadvantages of the spinner magnetometer are nonadaptability to the fitting of cooling and heating compartments around the sample for NRM temperature studies and disintegration of rock samples during the high speed rotation essential for higher levels of sensitivity.

The astatic magnetometer utilizes the principle of a magnetic suspension system which is insensitive to fluctuations in the neighboring magnetic field and reacts to the field gradient produced by a magnetic sample when situated in proper relationship within the system. A high degree of sensitivity is obtained by establishing a very weak controlling torque on the system. The magnetic system is comprised of diametrically opposed magnets attached to a very light rod suspended on a torsional fiber of minute cross section. The free period of oscillation of the suspension system determines the minimum time required for measurement of a single sample. The advantages of the astatic magnetometer are its high degree of sensitivity, if sufficient readings are taken it produces more accurate results than the spinner type for inhomogeneous and weak samples, lends itself to the addition of heating or cooling enclosures around the sample holder for studying temperature change effect on NRM. The disadvantages are its sensitivity to vibration, and humidity changes.

The ballistic method of NRM measurement operates on the principle of an electric charge produced as a result of relative motion between the rock sample and the pick-up coil. The electric charge produced by the change in magnetic flux through the coil is measured directly on a galvanometer. The advantage of the ballistic method is its adaptation to the measurement of large samples. The disadvantages of this instrument are its limited maximum sensitivity of approximately 1×10^{-4} emu/cm^3 and it is less convenient and less sensitive than the spinner magnetometer for measurement of weak NRM rocks and minerals.

The magnetic balance operates on the principle of measurement of the translational force exerted on the rock sample in a non-uniform magnetic field. The mechanical force exerted on the rock sample is determined by the sample volume and magnetization, the strength of the magnetic field and the field gradient. There are three different types of magnetic balances, namely the magnetic pendulum, spring balance, and vertical balance. Their operation differs from that of the astatic magnetometer which is a torque device, whereas the magnetic balance is a translational force device. The advantages of the magnetic balance are its ability to function over an extremely wide temperature range, its capabilities to measure not only remanent magnetization, but also to develop a complete hysteresis curve for ferromagnetic samples, to provide determination of the coercive force, paramagnetism or

diamagnetism of the sample, as well as its saturation magnetization. This makes it a highly versatile instrument. The instrument's principal disadvantage is the difficulty in the determination of absolute magnetization values, its sensitivity must be calibrated by means of a standard intensity sample.

The spinner magnetometer was selected in preference to the other types because of its high degree of measurement accuracy and stability, ease of operation, ability to adapt to various size samples and its freedom from the undesirable effects of vibration, and changes in temperature and humidity.

CHAPTER III

PRINCIPLE OF SPINNER MAGNETOMETER

The spinner magnetometer operates on the principle of the alternating current generator as described theoretically by Nagata (1961). The rock sample is rotated at a constant speed in proximity to a fixed pick-up coil, Figure 1, alternating electromotive force is induced in the pick-up coil by the rotating magnetic field developed by the component of magnetization perpendicular to the axis of rotation. The induced electromotive force is then electronically amplified and compared against a known reference signal for measurement.

The pick-up coil, Figure 1, is composed of a main coil L_1 around which a series balancing coil L_2 is concentrically wound in opposition to the main winding. The turns ratio of the two coils is designed so that when the coil assembly is placed in a uniform magnetic field "H" parallel to its axis the total effective magnetic flux Φ through each coil is equal.

This condition is expressed mathematically as

$$\Phi = \pi n^2 Hd\left(\int_{r_1}^{r_2} r^2 dr - \int_{r_2}^{r_3} r^2 dr\right) = \pi n^2 Hd(2r_2^3 - r_1^3 - r_3^3) = 0 \qquad (1)$$

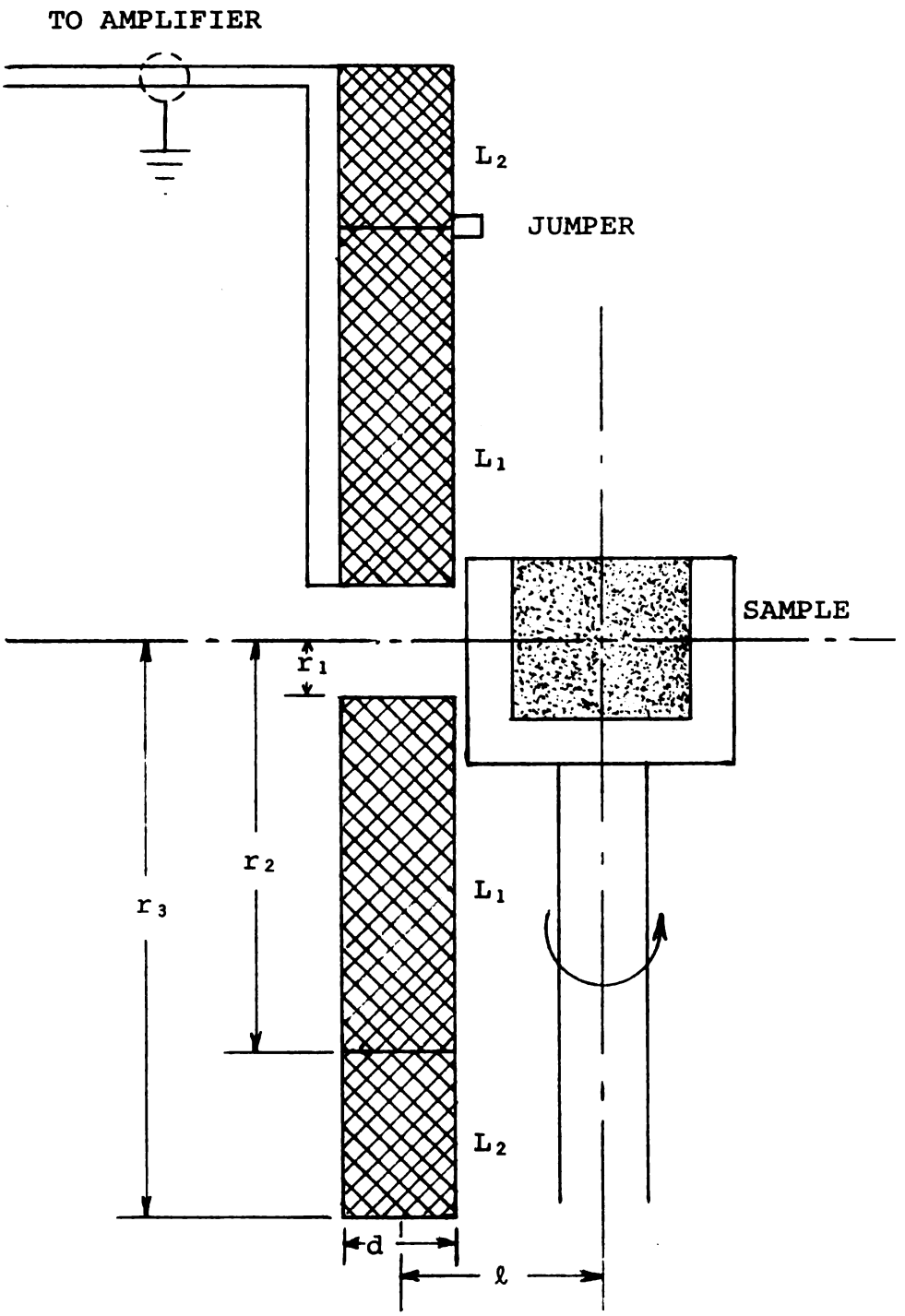

Figure 1. Schematic drawing of pick-up coil.

where d, n, r_1, r_2, and r_3 represent the thickness of the coil, the number of turns per cm, the inner radius of the mail coil L_1, the outer radius of the main coil L_1 which is equal to the inner radius of the balancing coil L_2 and the outer radius of the balancing coil L_2 respectively. The relationship for the coils radii is then

$$2r_2^3 = r_1^3+r_3^3. \tag{2}$$

Under this condition no magnetic induction is caused within the coil assembly as a result of changes occurring in a uniform magnetic field in which it is situated. This coil assembly also has the ability to eliminate the inductive effect due to mechanical vibration in the earth's magnetic field.

Assuming that the rock sample simulates a magnetic dipole, the magnetic potential W generated by the sample is given by

$$W = (\mu_x x+\mu_y y+\mu_z z)/R^3,$$

$$\mu^2 = \mu_x{}^2+\mu_y{}^2+\mu_z{}^2, \quad R^2 = x^2+y^2+z^2 \tag{3}$$

where the coordinates (x, y and z) are chosen so that the center of the magnetic dipole coincides with their origin. The quantity R represents the vector sum of the (x, y and z) coordinates and μ is the resultant permeability for an anisotropic sample with respect to its center. The axis of the coil assembly being taken as the z-axis and the

y-axis being taken as the axis of rotation of the sample.

The magnetic flux enclosed in an area of a single winding of the coil assembly is given by

$$\Phi = \int_0^r \int_0^{2\pi} H_z r dr d\theta = 2\pi\mu_z \frac{r^2}{(r^2+z^2)^{3/2}} , \tag{4}$$

where

$$H_z = \frac{\partial W}{\partial z} = \frac{\mu_z(r^2-2z^2)-3\mu_x rz \cos(\theta-\alpha)}{(r^2+z^2)^{5/2}} , \tag{5}$$

$$r^2 = x^2+y^2, \quad \tan\theta = y/x, \quad \tan\alpha = \mu_y/\mu_x.$$

Hence, the magnetic flux enclosed by the combined turns of the coil assembly is

$$\Phi = \int_{\ell-d/2}^{\ell+d/2} \frac{l}{D} \left\{ \int_{r_1}^{r_2} \phi dr - \int_{r_2}^{r_3} \phi dr \right\} dz \tag{6}$$

where ℓ is the mean distance between the dipole and the coil assembly and D is the effective diameter of the wire wound in the coil assembly.

In as much as the magnetic dipole is rotated at a constant speed about the y-axis,

$\mu_x = \mu_h \sin \omega t$, $\mu_z = \mu_h \cos \omega t$, where $\mu_h^2 = \mu_x^2+\mu_z^2$

and μ_y is a constant independent of time,

on the condition that an appropriate origin of time t is selected.

The electromotive force induced in the coil assembly as determined in equations (4), (5) and (6) by Nagata (1961) is expressed by

$$E = \frac{2\pi\omega}{D^2}\mu_h \sin \omega t \left[\ell \ln\left\{ \frac{r_1+\sqrt{r_1^2+(\ell-d/2)^2}}{r_1+\sqrt{r_1^2+(\ell+d/2)^2}} \cdot \left(\frac{r_2+\sqrt{r_2^2+(\ell+d/2)^2}}{r_2+\sqrt{r_2^2+(\ell-d/2)^2}} \right)^2 \right.\right.$$

$$\times \frac{r_3+\sqrt{r_3^2+(\ell-d/2)^2}}{r_3+\sqrt{r_3^2+(\ell+d/2)^2}} + \frac{d}{2} \ln\left\{ \frac{\left(r_2+\sqrt{r_2^2+(\ell+d/2)^2} \right)^2}{r_1+\sqrt{r_1^2+(\ell+d/2)^2}} \right.$$

$$\times \frac{\left(r_2+\sqrt{r_2^2+(\ell-d/2)^2} \right)^2}{r_1+\sqrt{r_1^2+(\ell-d/2)^2}} \cdot \frac{1}{r_3+\sqrt{r_3^2+(\ell+d/2)^2}}$$

$$\left.\left.\left.\times \frac{1}{r_3+\sqrt{r_3^2+(\ell-d/2)^2}} \right\} \right] . \qquad (7)$$

Therefore, the electromotive force which is generated is proportional to μ_h and can be appropriately amplified and measured.

Figure 2, illustrates diagrammatically, how the signal is processed and measured after being induced into the pick-up coil.

Figures 3 and 4 show the overall front and rear views of the magnetometer.

The signal from the pick-up coil is fed into the mixer where it can be transferred directly to the high gain amplifier through the band-pass filter to the oscilloscope for observation. The pick-up coil signal also can be combined with the reference generator signal, amplified

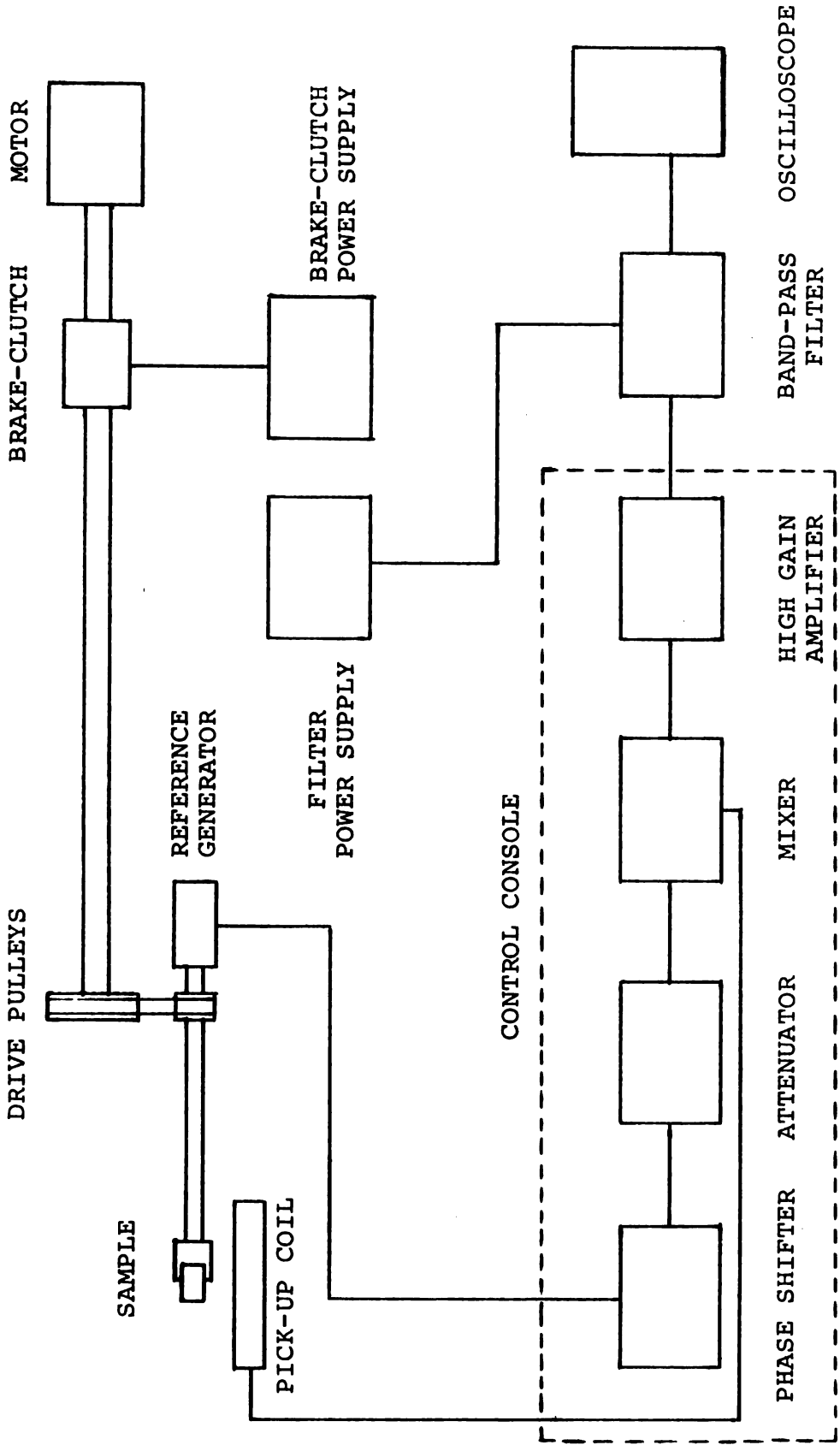

Figure 2. Block diagram of spinner magnetometer.

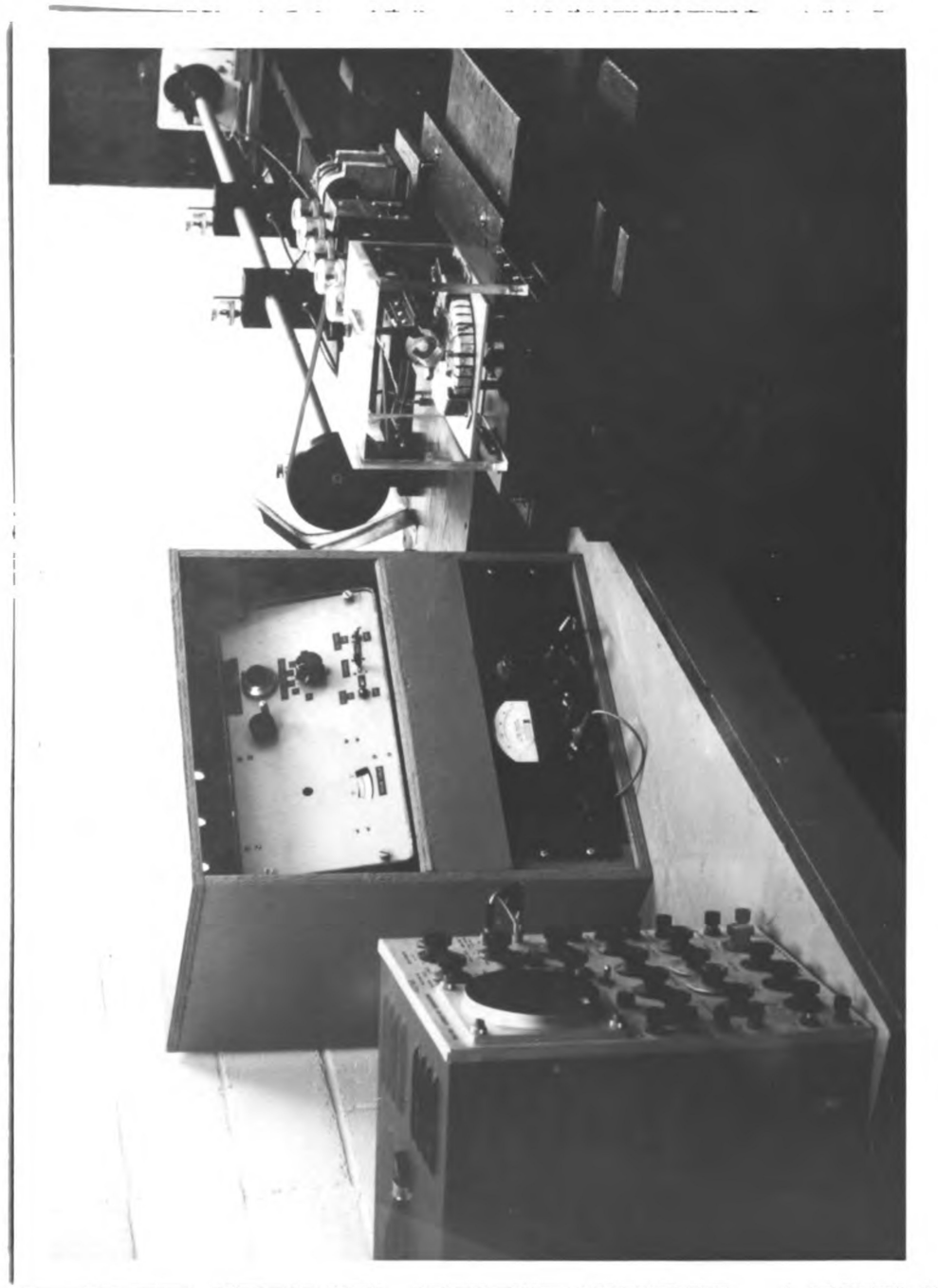

Figure 3. Front view of magnetometer.

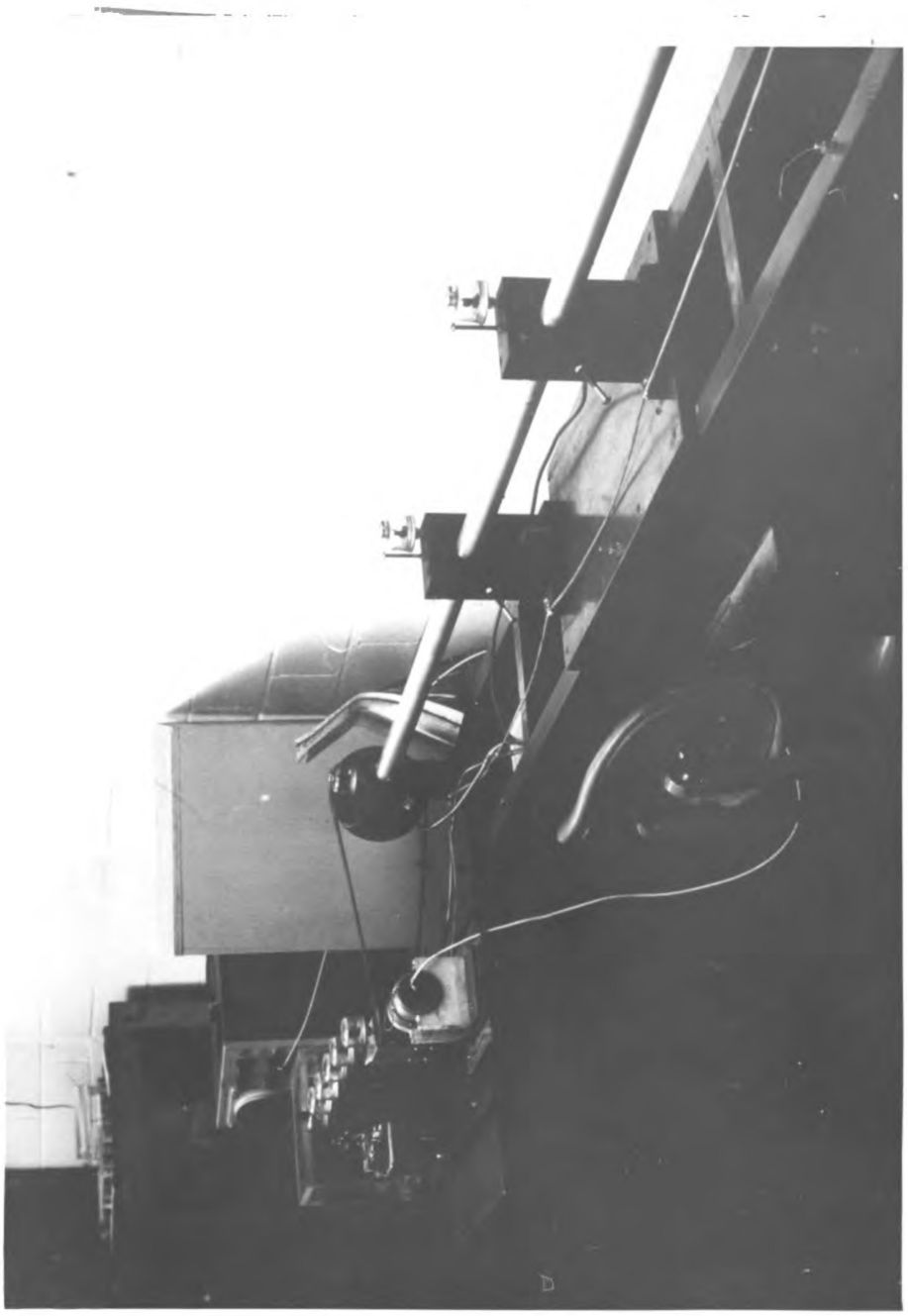

Figure 4. Rear view of magnetometer.

and filtered and observed on the oscilloscope. The signal from the pick-up coil can be eliminated, by grounding it out in the mixer, thus enabling the reference generator signal to be monitored independently.

A console serves as the control unit for the spinner magnetometer. It contains the brake-clutch switch, dial light switch, phase shifter, attenuator network, mixer circuit, and high-gain amplifier.

The unknown pick-up coil signal is compared with the reference generator signal of known phase and intensity. Measurement of the pick-up coil signal is accomplished by establishing a null or zero when it is combined with the reference generator signal. The null is achieved by simultaneously adjusting the phase and intensity of the reference signal to that of the pick-up coil signal by turning the rotor of the synchro receiver (phase shifter) and the decade attenuator (coarse intensity control) and ten turn potentiometers (fine intensity control) until the oscilloscope indicates zero output voltage.

In this instrument a synchro transmitter is used to generate the reference signal. The synchro transmitter energizes the synchro receiver which is utilized as the phase shifter. The theory of this synchro system which includes both transmitter and receiver is discussed below. The synchro transmitter and receiver each have stationary (stator) sets of windings. The stators and rotors are made of laminated sheet steel around which insulated copper

wire is wound to form the windings. The rotor of each unit has one winding and two salient (projecting) poles. The rotor winding is connected to two terminals identified as R1 and R2 in Figure 5 through carbon brushes in contact with two slip rings. The stator of each unit has three windings which are wound in slots in the cylindrical laminations, 120 degrees apart. A single stator winding (coil A) and the rotor winding are shown in Figure 5. The turns of coil A lie in planes perpendicular to the axis of this stator coil, marked "axis of coil A." This axis indicates the direction of the magnetomotive force developed when current flows in coil A. The three stator windings in this instrument are connected in a delta connection, as shown in Figure 6. The stator terminals are identified as S1, S2, and S3, as shown in Figure 6. The terminal numbers increasing in the counter-clockwise direction about the stator (when viewing the shaft end of the machine). In this system the corresponding stator terminals of transmitter and receiver making up the synchro system are connected together. The rotor terminals of the transmitter are left disconnected to utilize the residual magnetism of the rotor to excite the generation of the electromotive force in the transmitter. The rotor terminals of the receiver (phase shifter) are connected to the input of the attenuator network within the control console. The wiring configuration used between transmitter and receiver stator terminals cause the development of a magnetic field in the

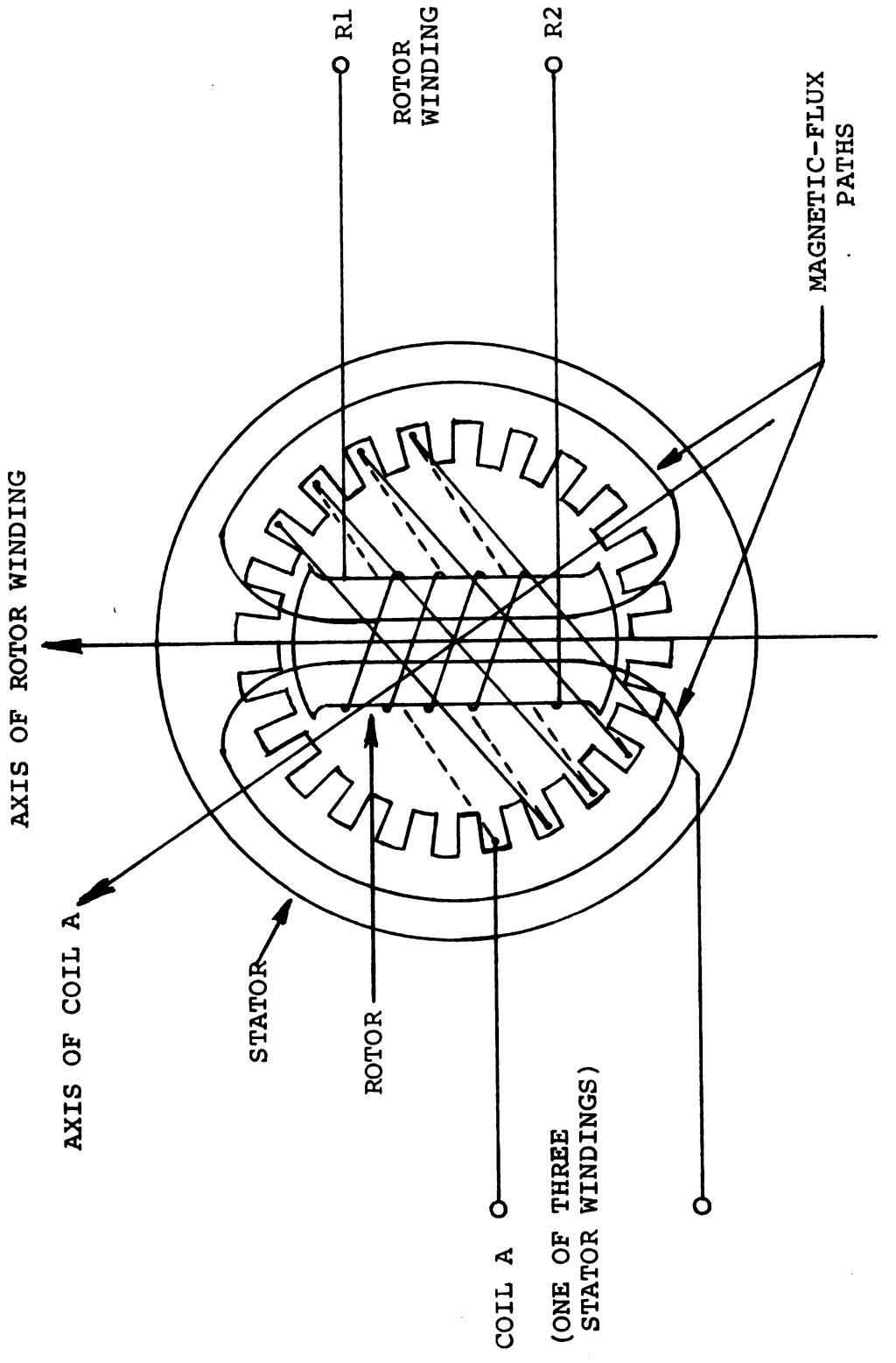

Figure 5. Cross section of a synchro unit.

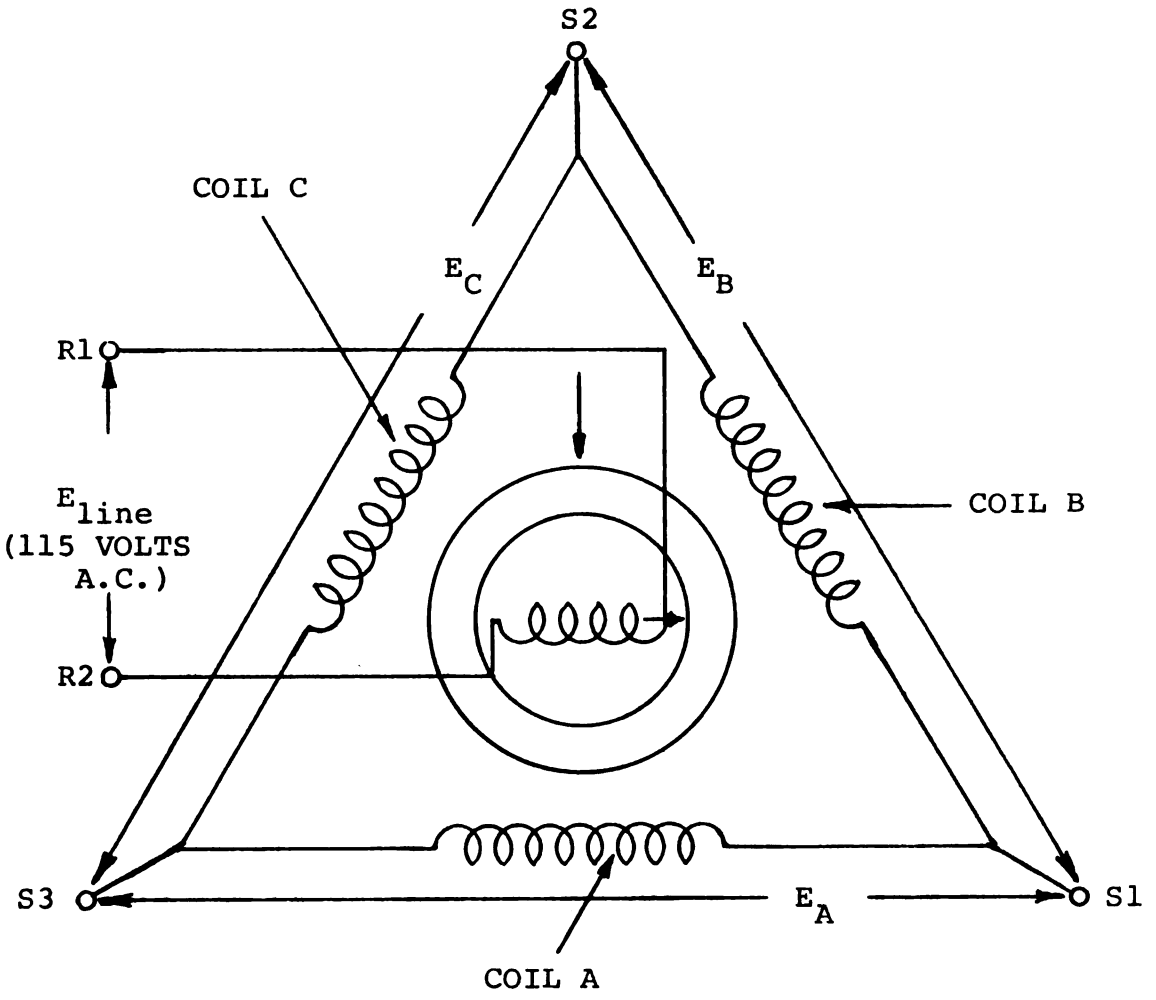

Figure 6. Rotor and stator voltages of delta-connected synchro.

stator of the synchro receiver identical to the magnetic field produced in the stator of the synchro transmitter. The residual magnetism of the rotor of the transmitter produces a magnetic flux approximating that shown in Figure 5. When the rotor is rotated this flux induces alternating voltages in the stator windings of the transmitter. In this respect the synchro is similar to a single-phase transformer with the rotor winding forming the primary and the stator winding representing three secondary windings.

The amplitudes of the electromotive forces induced in the stator windings depend upon the number of relative turns on the rotor and stator windings and the orientation of the rotor. The position of the rotor as illustrated in Figure 6 will induce a maximum amplitude (in phase) electromotive force E_A across coil A, since maximum magnetic flux from the rotor is cutting through coil A. If the rotor is rotated clockwise from the position shown in Figure 6 E_A decreases and falls to zero as the rotor axis becomes perpendicular to the axis of coil A. Further clockwise rotation of the rotor causes a voltage of opposite phase to develop across coil A. The variation of the root mean square (rms) electromotive force E_A with the angular position of the rotor is presented graphically in Figure 7, after Reintjes and Coate (1952). This figure represents the stator voltages developed with 115 volts, 60 cycles excitation voltage applied to the rotor winding. The maximum rms voltage developed in this instrument is

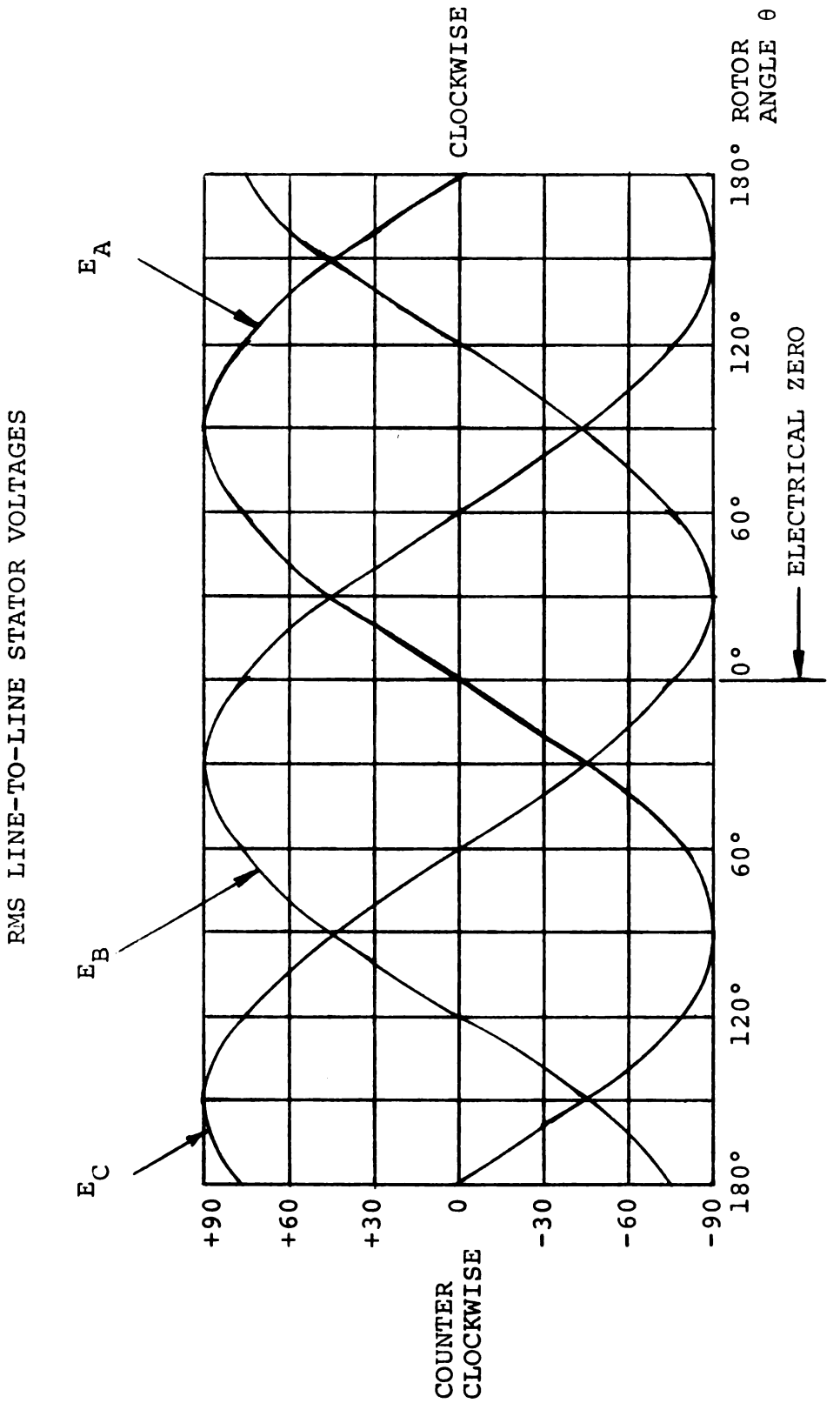

Figure 7. Root mean square voltages as functions of rotor angle θ.

slightly more than 9 volts, since no excitation voltage is applied to the rotor winding. The 9 volts output is generated as a result of the residual magnetism of the rotor.

The rotor angular position is normally taken with respect to a standard position designated electrical zero. Electrical zero is the position of the rotor for which the voltage between S1 and S3 is zero, and the voltage at S2 (with respect to S1 or S3) is in phase with the excitation voltage at R1 (with respect to R2). The conventional representation of the electrical zero position on synchro diagrams is shown by an arrow directed from R2 toward R1 along the rotor axis and another arrow located on the stator so that the arrows coincide at the electrical zero position as shown in Figure 6. The rotor angle θ is used in plotting the loci in Figure 7.

The rotors orientation shown in Figure 6, corresponds to $\theta = 90$ degrees clockwise and is so plotted in Figure 7. In phase relationships between E_A and the excitation voltage (E_{line}) applied to the rotor are shown as positive values of E_A in Figure 7. Negative values of E_A indicate a 180 degree out-of-phase relationship between E_A and E_{line}.

The distribution of the windings in the stator slots and the shape of the rotor pole faces have to be carefully designed to produce a sinusoidal variation in the rms value of E_A. The loci of the voltages across coils B (E_B) and C (E_C) are also of the same sinusoidal shape. The

orientation of the stator coils causes a 120 degree displacement between the loci of the voltages produced by any two stator coils as shown in Figure 7. The point-by-point addition of the ordinates of the three (3) loci produces a sum of zero for E_A, E_B, and E_C for each position of the rotor. Thus no appreciable circulating current will flow if the delta is formed into a closed loop as shown in Figure 6.

In this system the coresponding stator terminals of transmitter and receiver are connected together. The rotor terminals of the transmitter are left disconnected. The rotor terminals of the receiver are connected to the input of the attenuator. The voltages induced in the transmitter stator windings when its rotor is turned, applies these same voltages to corresponding stator windings of the receiver causing current to flow in these windings setting up magnetic flux in the receiver. This arrangement produces a self-induced voltage developed by the flux in the respective receiver stator windings equal to the voltage induced by the flux in the corresponding transmitter stator windings, neglecting resistance of the windings. Since the windings in the transmitter and receiver are essentially identical, the equal fluxes in the corresponding windings produce equal voltages, thus the orientation of the magnetic field in the receiver must be identical with the magnetic field in the transmitter. In summary, the set of three stator voltages from the

transmitter serve as signal voltages which cause the development of a magnetic field in the receiver in a direction parallel to that set up by the transmitter rotor. Therefore if the transmitter and receiver making up the synchro system are each carefully set at electrical zero the receiver can be used as an indicator to show the exact angular position of the transmitter rotor.

In this instrument the rotor of the transmitter is mechanically set on a common drive shaft with the sample holder as shown in Figure 8 so that the zero degree phase position of the sample holder coincides with the electrical zero setting of the transmitter. The synchro receiver is also set at the electrical zero of the transmitter. The receiver is mounted on the console panel and carefully fitted to an accurately calibrated 0 to 360 degree dial which is used to indicate the exact angular position of the sample holder for direct readout of the phase angle of the rock sample placed in the holder.

The schematic diagram of the phase shifter, attentunator network and mixer circuit is shown in Figure 9. The attenuator network consists of a fine intensity control and a coarse intensity control. The fine intensity control circuit is comprised of a resistive network of R1, R2, R3, R4 and R5. Two ten-turn linear potentiometers, R2 (500 ohms) and R3 (300 ohms) which are ganged on a common (fine intensity) control shaft vary the voltage across R5 (550 ohms) by a factor of 1 to 0.1. A three-digit

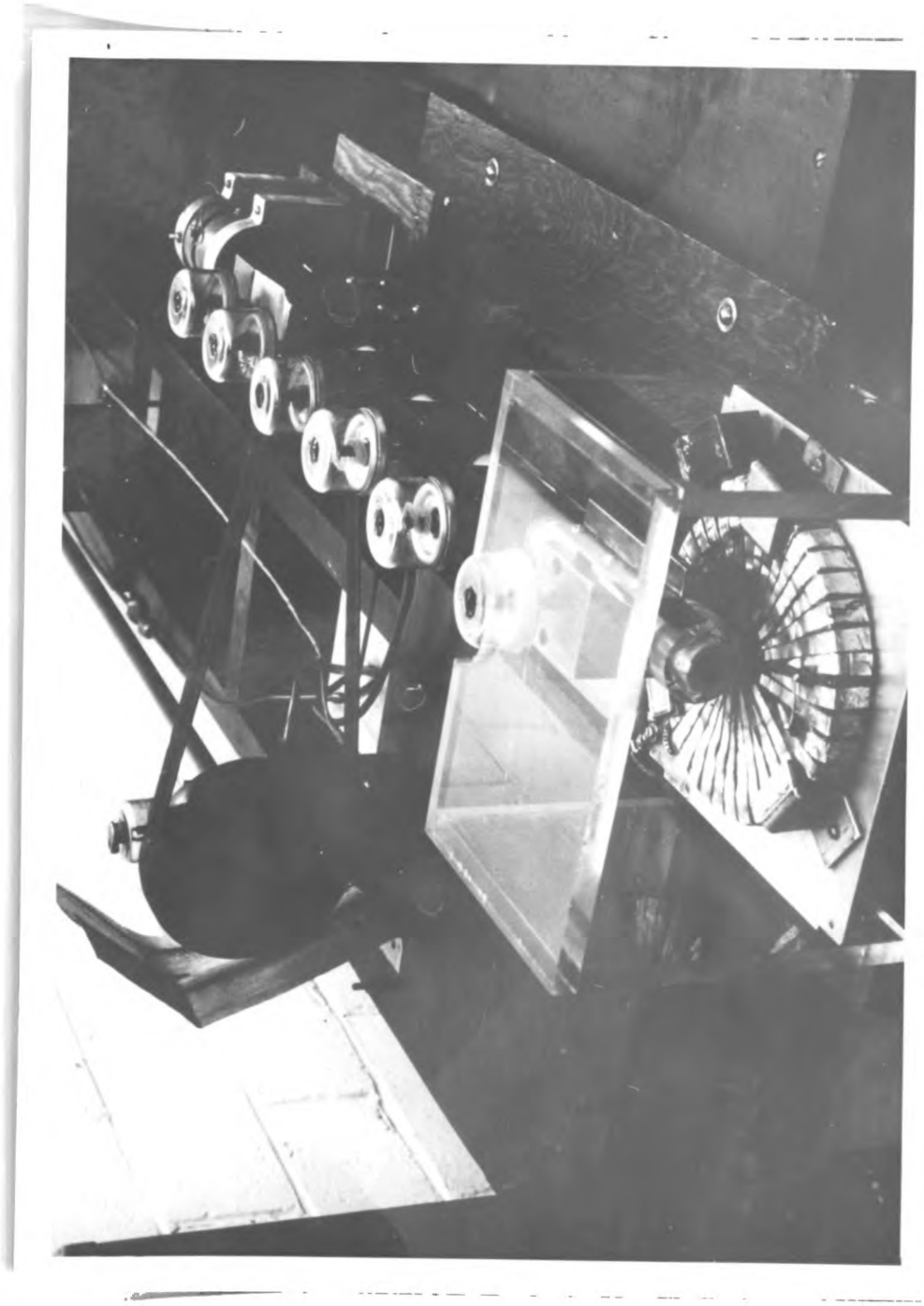

Figure 8. Oblique view of spinner shaft.

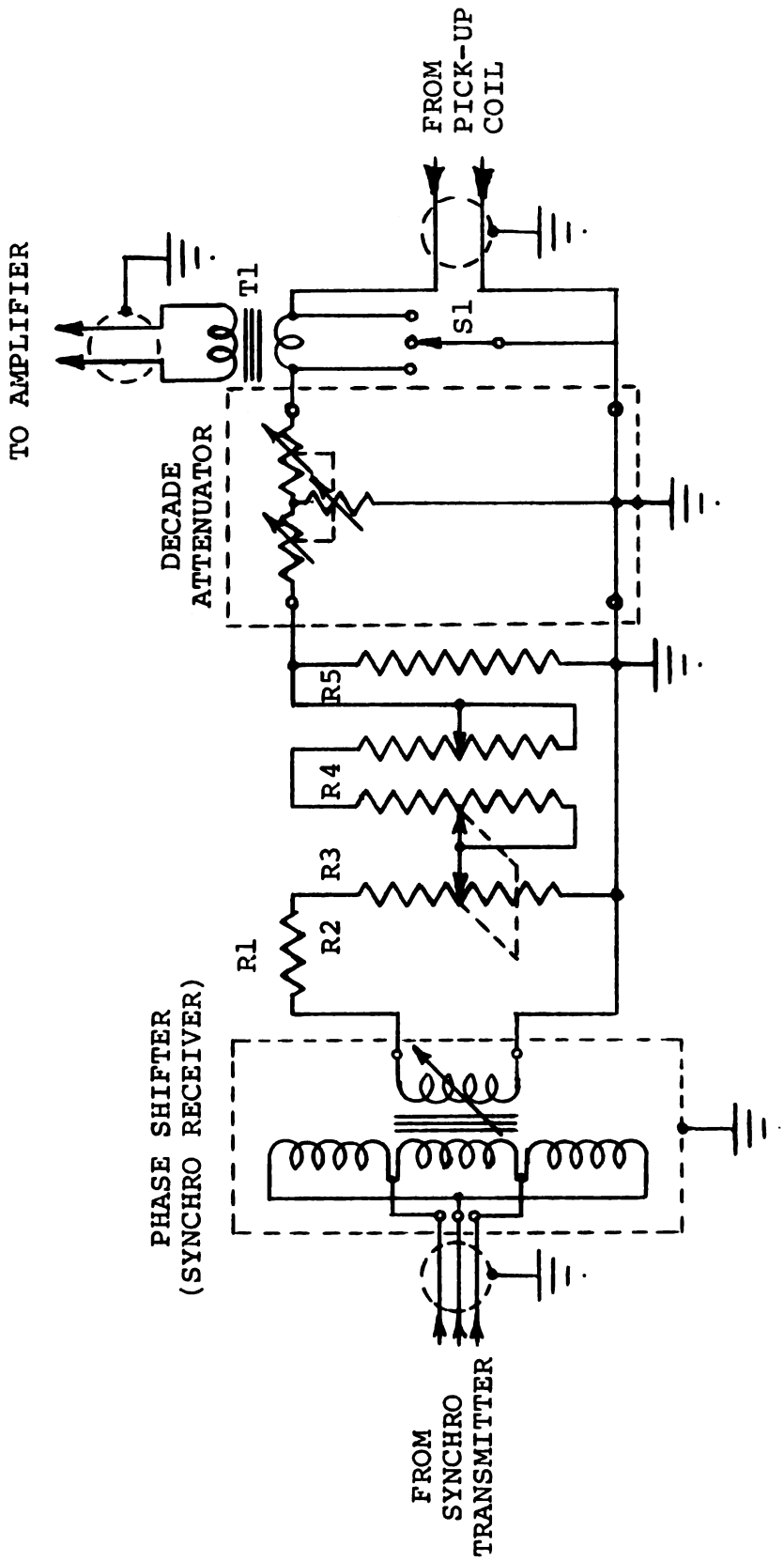

Figure 9. Schematic diagram of phase shifter, attenuator, and mixer circuits.

ten-turn dial is used as the fine intensity control which actuates the ganged potentiometers. The coarse intensity control is comprised of a single five-step commercial type T voltage attenuator (600 ohm impedance) that has a range of 0 to 100 db (decibel) in 20 db steps. This device enables adjustment of the output voltage to 1 per cent of its value. Voltages as small as 1×10^{-6} of full value may be obtained at the output of the decade attenuator.

The attenuator network contains a calibrating resistor R4 (5,000 ohms) which is used to calibrate the attenuator to read directly in emu (electromagnetic units) between 1.00×10^{0} and 10.00×10^{-5}, to three-digit accuracy.

The mixer circuit consists of a single pole triple throw switch and a matching transformer with a primary impedance of 125 ohms and a secondary impedance of 39,000 ohms. The turns ratio of the transformer is 1:18. The switch S1 (Figure 9) provides a means of observing the pick-up coil signal, the reference generator signal at the output of the decade attenuator or these two signals combined. These two signals are combined in the primary of the mixer transformer, this is the normal mode of operation of the instrument and is obtained by placing switch S1 in the neutral position. The secondary winding of the mixer transformer is connected to the input terminals of the high-gain amplifier. The output of the amplifier is connected to the input of the band-pass filter. Details on

the band-pass filter are presented in Doell and Cox (1965). The filter is adjusted to pass the operating frequency of the instrument, 100 cps in this case, and reject unwanted noise frequencies on either side of the operating frequency. This adjustment is made by four controls mounted on the band-pass filter panel, see Figure 10. Two of these controls which are attached to two ganged potentiometer each adjust the band-pass center frequency, one control for coarse and the other for fine adjustment. The other two controls adjust the selectivity (width) of the band-pass, one potentiometer being the coarse adjustment and the other the fine.

The output of the band-pass filter is connected to the vertical input of an oscilloscope which is used to observe the output signals of the instrument.

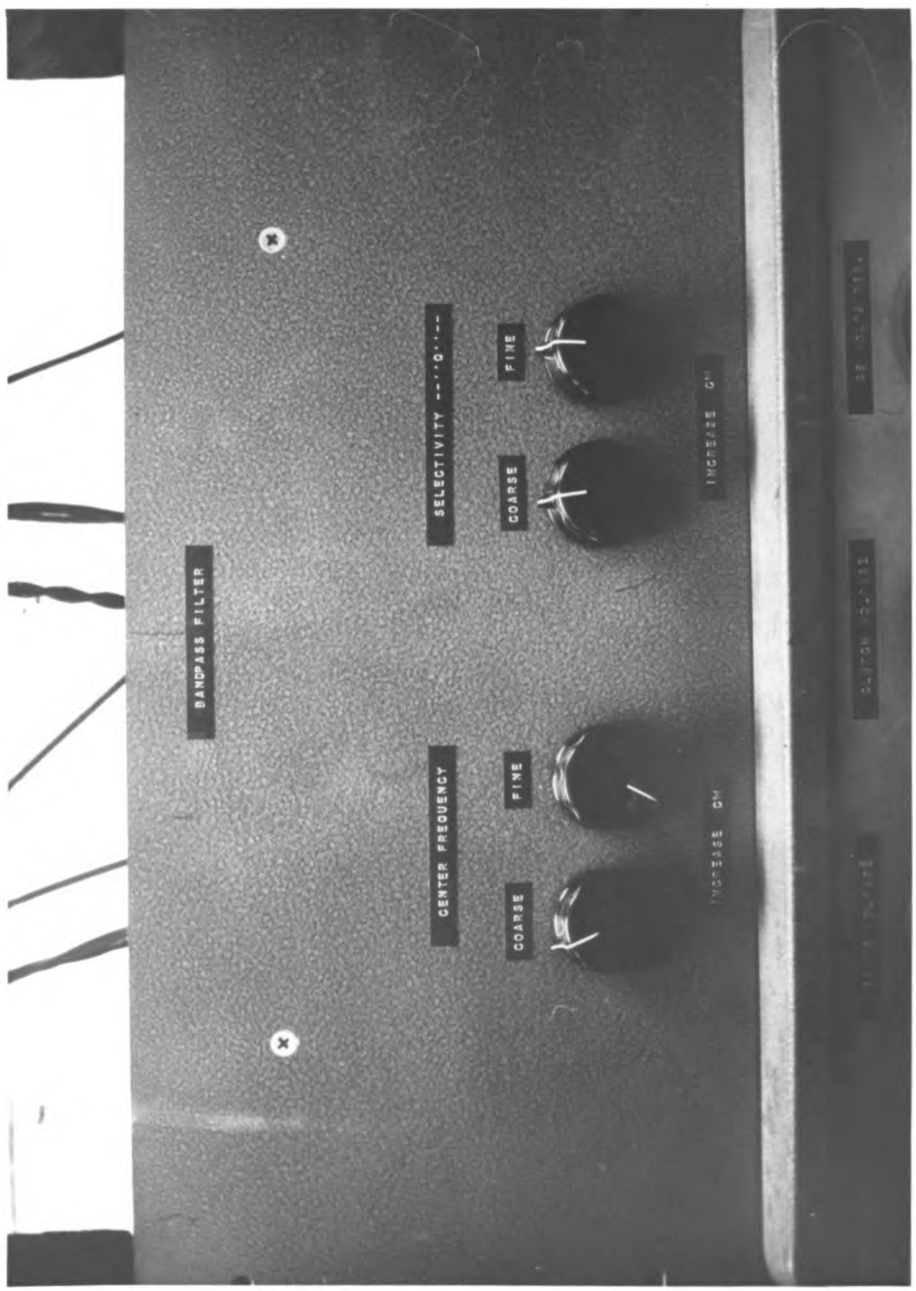

Figure 10. Band-pass filter.

CHAPTER IV

DESIGN OF SPINNER MAGNETOMETER

The design considerations of the constructed instrument are the same as those developed by Doell and Cox (1965) except for the modifications discussed below.

The drive mechanism has been improved by the use of a one-half horsepower, 1725 revolutions per minute, 60 cycle, alternating current, induction motor, thus providing greater speed stability, particularly with the larger size sample holders.

A magnetic brake-clutch, Sterns Electric Corporation model 3CFCB, 90 volts direct current was inserted in the drive mechanism by mounting it directly on the shaft end of the motor, Figure 11. A brake-clutch power supply, Figure 12, was designed to control both clutch engagement time and the brake application time. This unit provides greater flexibility in control of the starting and stopping action of the spinner shaft for various sizes of sample holders. It also permits the motor to run at a constant speed continuously. This innovation greatly improves the efficiency of the instrument since it eliminates the need to wait for

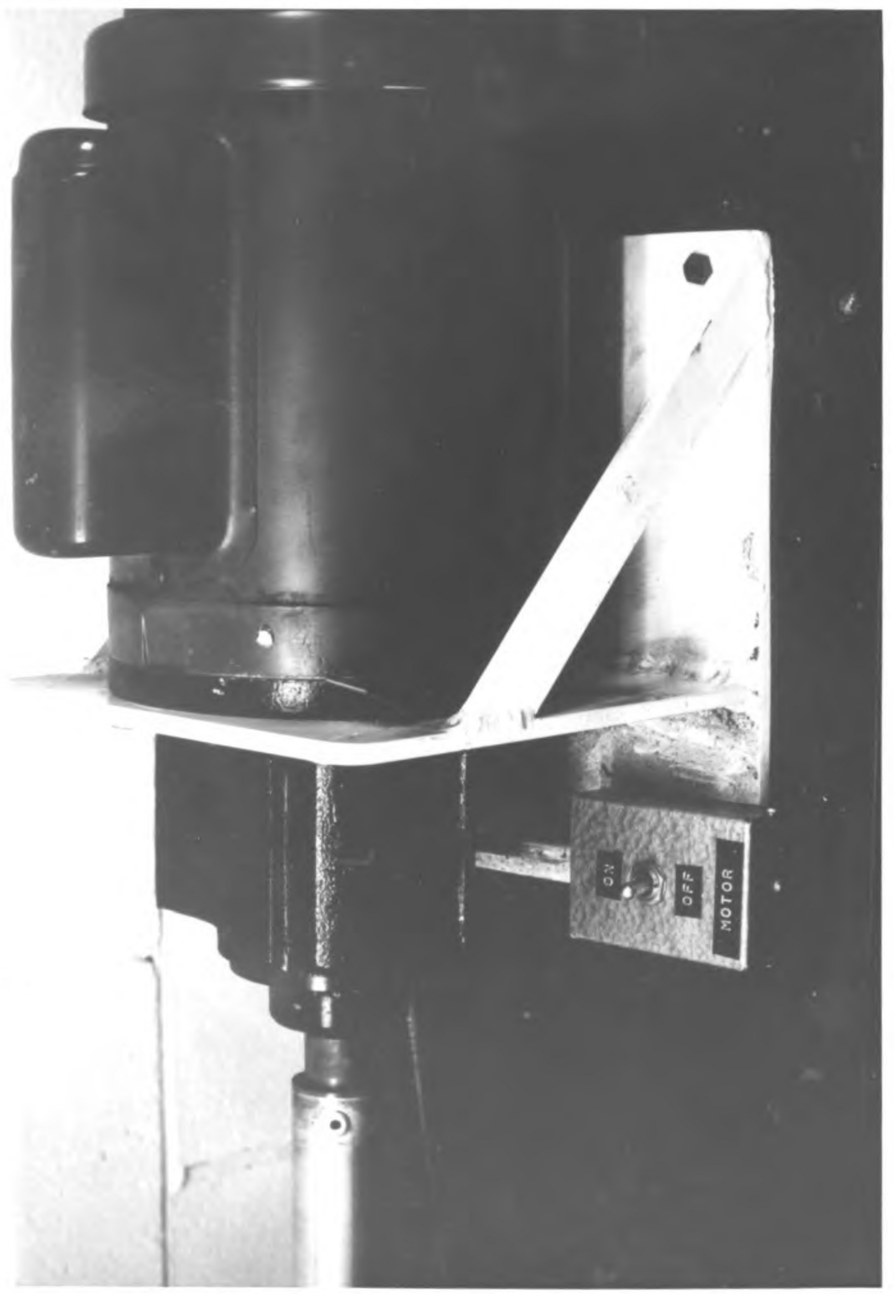

Figure 11. Drive motor, brake-clutch, and switch.

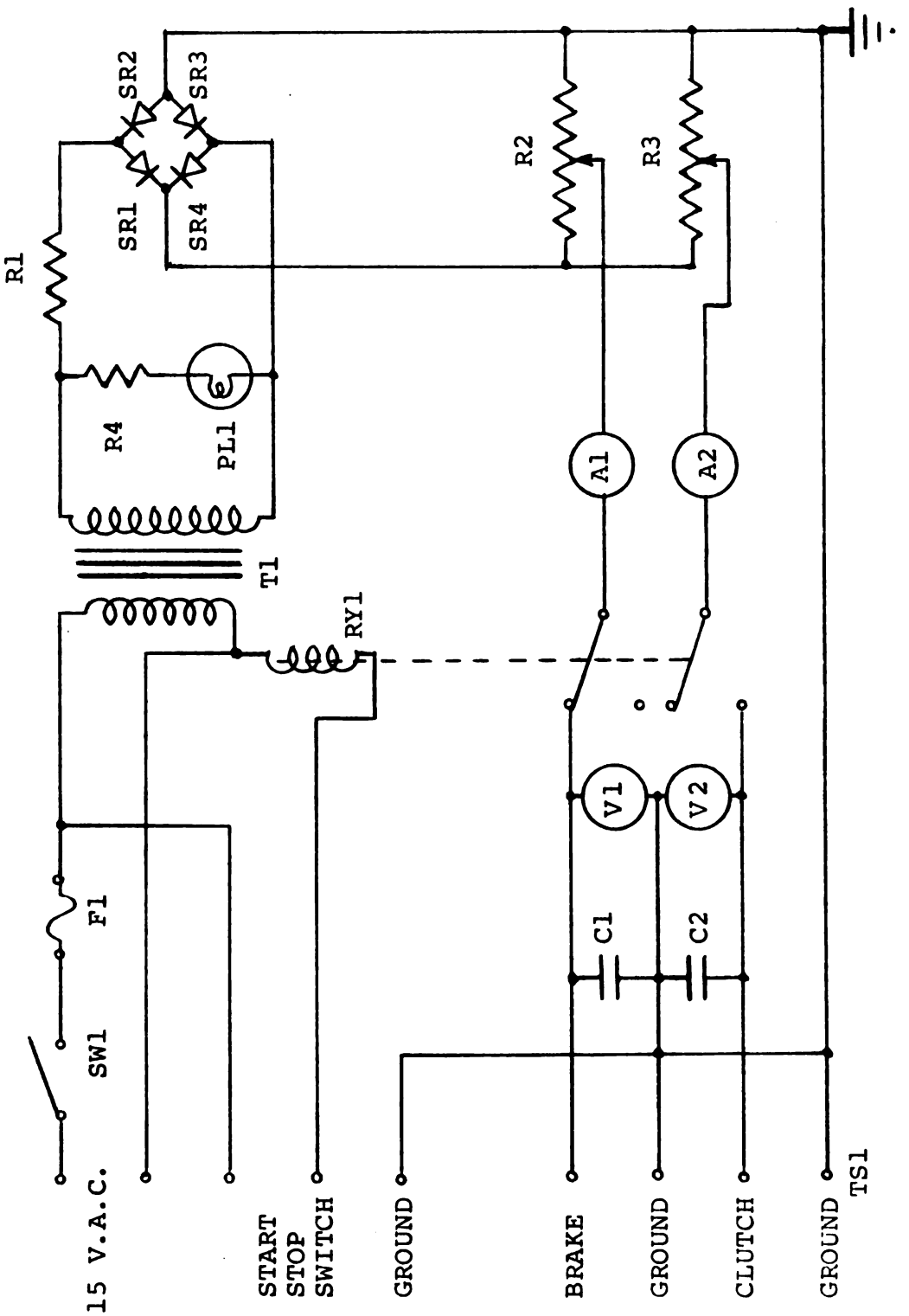

Figure 12. Schematic diagram of brake-clutch power supply.

the motor to reach normal operating speed or to come to a stop.

Considerable modification of the spinner shaft assembly was necessary to retain stability of the instrument when the larger size spinner heads and sample holders were rotated. Figure 8 shows the principal modifications made to include: a large magnesium spinner shaft bed, six oil lubricated bearings, a one-inch diameter nylon spinner shaft in place of the three-quarter-inch shaft of the prototype instrument.

The drive pulley ratio was changed to provide a spinner shaft velocity of 6,000 RPM. This was necessary to provide the desired 100 cycles per second operating frequency for the instrument. This frequency of operation was chosen to provide better frequency separation between it and the 60 CPS electrical power frequency and particularly its second harmonic of 120 CPS. Also 100 CPS filters are more readily available than those designed for odd frequencies.

Figure 8 also shows the polonium 210 electrical static eliminator used to neutralize the static charge developed on the spinner head when the instrument is in operation. The radioactive polonium 210 emits high velocity alpha rays which ionize the air in the vicinity of the spinner head. The ions produced dissipate the static electrical charge.

The sample system designed for this instrument consists of four separate spinner heads which may be installed on the spinner shaft for measurement of any one of four standard drill core size samples, Figure 13. A cubical sample holder has been made which fits into its respective spinner head for core sizes shown in Table 1.

A mechanical elevating stage, Figure 14, was designed to position the pick-up coil for each sample holder.

The reference system of the instrument has been modified by the use of a synchro transmitter as the reference generator in place of the 12 coil, two bank unit used in the prototype instrument. This change eliminated the need for astaticising the disc magnets of the reference generator rotor. Measurements made with the signal switch in "sample" position have shown that there is no observable noise signal induced into the pick-up coil by the magnetic field produced by the rotor of the synchro transmitter.

The measuring system of the instrument is electrically the same as the original instrument except for the substitution of the synchro transmitter for the reference generator. The synchro transmitter produces the reference signal against which the unknown signal developed by the rock sample in the pick-up coil is compared for measurement purposes. The phase of the synchro transmitter (reference) signal is known by direct readout of the phase angle indicator after being calibrated as described later.

Figure 13. Four sizes of sample holders and spinner heads.

TABLE 1.--Drill core sample holder dimensions.

Series	Diameter of Core	Length of Sample	Holder Bore Diameter	Holder Depth of Bore
EX	0.875	0.802	0.880	0.810
1"	1.000	0.916	1.005	0.925
AX	1.275	1.167	1.280	1.177
BX	1.625	1.488	1.630	1.500

Dimensions in inches

Ratios: Diameter/Length = 1.092

Length/Diameter = 0.916

Figure 14. Elevating stage, pick-up coil and spinner head.

The intensity of the reference signal is also known and is read directly from the coarse and fine intensity controls after being calibrated as described later.

CHAPTER V

CALIBRATION AND PRECISION OF MAGNETOMETER

In order to make the magnetometer operational, it is necessary to align and calibrate it. This requires adjusting the rotation of the spinner shaft to the desired velocity and aligning the band-pass filter to the desired frequency. The instrument was then calibrated to a selected secondary standard sample and the linearity of the intensity calibration was checked by the current coil method. The phase angle measuring system was aligned by comparing the reference system against the phase angle dial. The calibration of both phase and intensity was checked by comparison of measurements on samples studied at other laboratories. The internal consistency of measurements made with the magnetometer was tested by replication.

During the construction of the drive mechanism it was necessary to adjust the pulley ratio to attain the proper rotation speed of 6,000 revolutions per minute (RPM) of the spinner shaft. This was accomplished by using a General Radio Type 1531-A Strobotac, electronic stroboscope

to measure the speed of rotation of the spinner shaft. The small spinner shaft drive pulley diameter was re-machined until the 6,000 RPM speed was attained, thus producing an operating frequency of 100 CPS for the instrument.

The band-pass filter was aligned to a center frequency of 100 CPS using a Hewlett Packard, Model 650A Test Oscillator as a signal generator and a Tektronix, Type 564B oscilloscope as an output voltage indicator. The band-pass filter was then adjusted to provide the sharpest selectivity response curve (smallest band-pass width) by a trial and error process. This was accomplished by following the alignment procedure for the band-pass filter given by Doell and Cox (1965).

The intensity of the magnetometer was calibrated to the +Z axis of sample 1C101-1 supplied by the U.S. Geological Survey, Branch of Regional Geophysics, located at Menlo Park, California. This axis has a magnetic moment of 1.67×10^{-2} emu or an intensity of 1.47×10^{-3} emu/cm^3 as measured by the laboratory. This was accomplished by setting the fine attenuator control at 1.67 and the coarse attenuator control at 10^{-2} emu and adjusting the calibrating resistor R4, Figure 9, until a null was obtained. The calibrating resistor is used to calibrate the fine attenuator control.

The linearity of the intensity calibration was checked by using the current coil method suggested by Doell and Cox (1965). The block diagram of this method is

illustrated in Figure 15. The pick-up coil was removed from the adjustable stage of the instrument and replaced by an auxiliary coil. The signal coupled into the auxiliary coil by the magnetic field of a rotating small magnet mounted in the sample holder is amplified and applied to a test coil. The test coil is mounted on top of the pick-up coil into which the calibrating signal is induced, as a result of the current flow in the test coil. The current through the test coil was measured by means of an oscilloscope used to determine the voltage drop across a precision resistor in series with the coil. The method provides better accuracy of alternating current measurement than the ammeter method used by Doell and Cox. The pick-up coil and test coil had to be removed beyond the field of the small magnet placed in the sample holder of the magnetometer to prevent introduction of a noise signal into the calibration system. The signal induced by the test coil into the pick-up coil is measured on the magnetometer in the normal operational manner. A range of known intensity signals can be coupled into the pick-up coil by using the decade resistance as a control.

The linearity of the magnetometer was checked over the range of the fine attenuator control using this arrangement. The auxiliary coil and test coil were wound to the specifications given in Doell and Cox (1965). The actual signal induced by the test coil can be calculated to the degree of accuracy of the test coil's physical measurements.

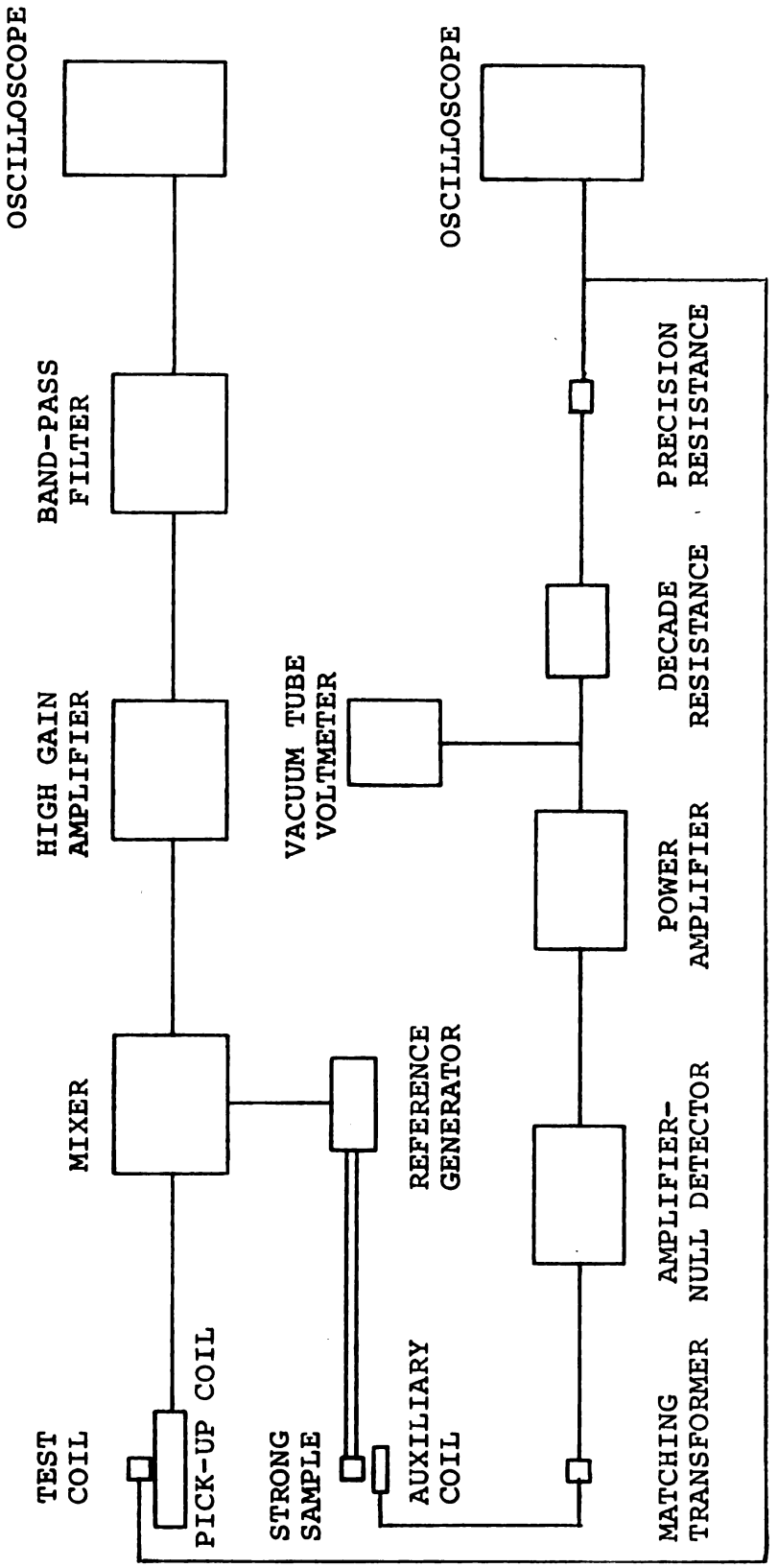

Figure 15. Block diagram of current coil calibration method.

The results of this test are shown in Figure 16. The figure illustrates good linearity over the range 1 x 10^{-2} through 4 x 10^{-1} emu. The slight offset of the curve below 10^{-2} emu may reflect the errors in the voltage measurements due to limited current through the precision resistance.

The phase calibration was undertaken as outlined below: the syncro transmitter and receiver were each set and aligned to each other at electrical zero, as described previously in Chapter III. The phase angle dial was then set on the shaft of the synchro receiver so that the zero degree calibration on the dial coincided with the electrical zero of the synchro receiver. The spinner head was then set on the spinner shaft so that its zero degree index mark coincided with the electrical zero of the synchro transmitter mounted on the same shaft. The phase angle dial of the synchro receiver reads directly the angular position with regard to the zero degree index on the spinner head. The Z axis is accurately scribed on the cubical sample holder so that the Z axis marked on the rock sample can be aligned to it when the sample is placed in the holder. The X and Y axes are also scribed on the cubical sample holder so that any one of the three axes may be aligned with the index on the spinner head, permitting measurement of phase angle for each axis. The axial indexes on the cubical sample holder are marked with an arrow head pointing in the positive axial direction to

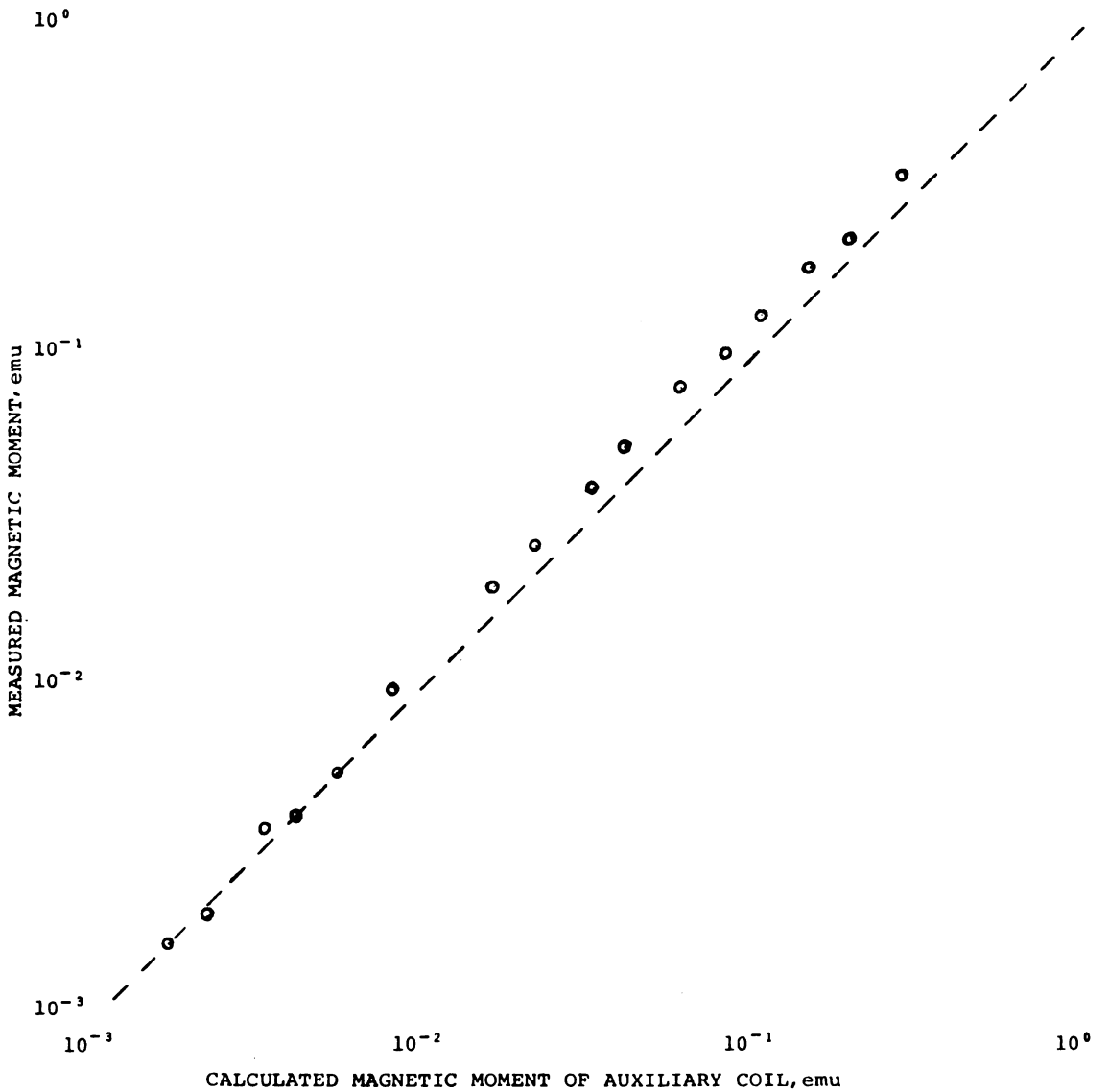

Figure 16. Intensity linearity test.

enable insertion of the holder into the spinner head for reading either positive or negative axial spins. This arrangement permits the six-spin procedure to be accomplished efficiently.

The linearity of the phase calibration was checked using a cubical sample holder with machine indexed holes drilled at 15° increments. A plastic cylinder was fitted with a needle magnet centered perpendicular to the axis of rotation and an indexing pin to fit into the above nolder. This device was used to check the accuracy and linearity of the phase angle measuring system by use of repeated measurements. The accuracy was found to be well within one degree with excellent linearity.

The accuracy of the calibration was cross-checked with a suite of samples ranging in intensity from 10^{-1} to 10^{-5} emu/cm^3. This suite includes samples provided by Dr. Richard Doell of the U.S. Geological Survey, Branch of Regional Geophysics, Menlo Park, California; Dr. LeRoy Scharon of the Earth Science Department, Washington University, St. Louis, Missouri; and the Geophysics Laboratory, Michigan State University.

Table 2 tabulates the comparison of measurements made by the U.S. Geological Survey on these samples with those made on the M.S.U. magnetometer. This table also shows a comparison with a sample measured at Washington University.

TABLE 2.--Comparison of measurements with other instruments.

Sample	Instrument	MSU	USGS	WU	Deviation	
	Date	3-25-70	2-9-70	3-20-68	USGS	WU
WU	Dec. deg.	247.0	242.9	245.4	-4.1	-1.6
PK5E	Inc. deg.	69.8	69.5	70.3	-0.3	+0.5
	Int. x 10^{-3}	1.17	1.11	1.33	-0.06	+0.16
	Date	2-6-70	2-9-70			
USGS	Dec. deg.	132.3	138.7		+6.4	
OC078-1	Inc. deg.	33.7	33.2		-0.5	
	Int. x 10^{-4}	1.33	1.47		+0.14	
	Date	2-6-70	2-9-70			
USGS	Dec. deg.	139.2	144.7		+5.5	
1C101-1	Inc. deg.	18.5	18.7		+0.2	
	Int. x 10^{-3}	1.51	1.59		+0.08	
	Date	2-6-70	2-9-70			
USGS	Dec. deg.	333.2	337.7		+4.5	
4D213-1	Inc. deg.	- 5.4	- 1.0		+4.4	
	Int. x 10^{-5}	3.58	4.44		+0.86	
	Date	2-11-70	2-9-70			
MSU	Dec. deg.	144.6	145.6		+1.0	
CS-1	Inc. deg.	6.8	6.8		0.0	
	Int. x 10^{-2}	3.26	3.63		+0.37	
	Date	2-11-70	2-9-70			
MSU	Dec. deg.	321.7	320.9		-0.8	
CS-2	Inc. deg.	23.6	20.8		-2.8	
	Int. x 10^{-3}	5.85	5.62		-0.23	
	Date	2-11-70	2-9-70			
MSU	Dec. deg.	151.5	151.7		-0.2	
CS-4	Inc. deg.	-23.5	-22.9		+0.6	
	Int. x 10^{-4}	5.24	5.86		+0.62	
	Date	4-8-70	2-9-70			
MSU	Dec. deg.	194.7	191.1		-3.6	
VN18D-1	Inc. deg.	-33.9	-40.5		-6.6	
	Int. x 10^{-5}	1.09	1.07		-0.02	
	Date	4-8-70	2-9-70			
MSU	Dec. deg.	272.9	273.4		+0.5	
YR9F-1	Inc. deg.	-23.3	-27.7		-4.4	
	Int. x 10^{-5}	1.59	1.35		-0.24	

Figures 17, 18, and 19 compare the intensity, declination and inclination of the M.S.U. measurements against those of other laboratories. The dashed line on each of the figures represents coincidence of instrument reading. If the plotted point is above the line, the M.S.U. instrument is reading higher than the other instrument. If the point is below, it is reading lower than the other instrument. The measurements as shown in Figures 17, 18, and 19 and tabulated in Table 2, show excellent correlation. The maximum error in declination and inclination are respectively 6.4 and 6.6 degrees. The maximum error in intensity within any decade unit which is controlled by the calibration resistor is 0.86. The standard deviation of the declination and inclination measurements are respectively 3.7 and 3.2 degrees and for the intensity, disregarding the decade unit, is 0.39 emu/cm^3. These values represent the relative calibration error with respect to the other laboratories plus several other possible sources of error.

The soft magnetic components within a sample may change with time. Therefore the NRM of samples may change during the time the samples are in transit between laboratories. The magnitude of this error may be evaluated by the change in the measurements of the three U.S. Geological Survey samples from the time they left the laboratory until their return. The intensity changes observed

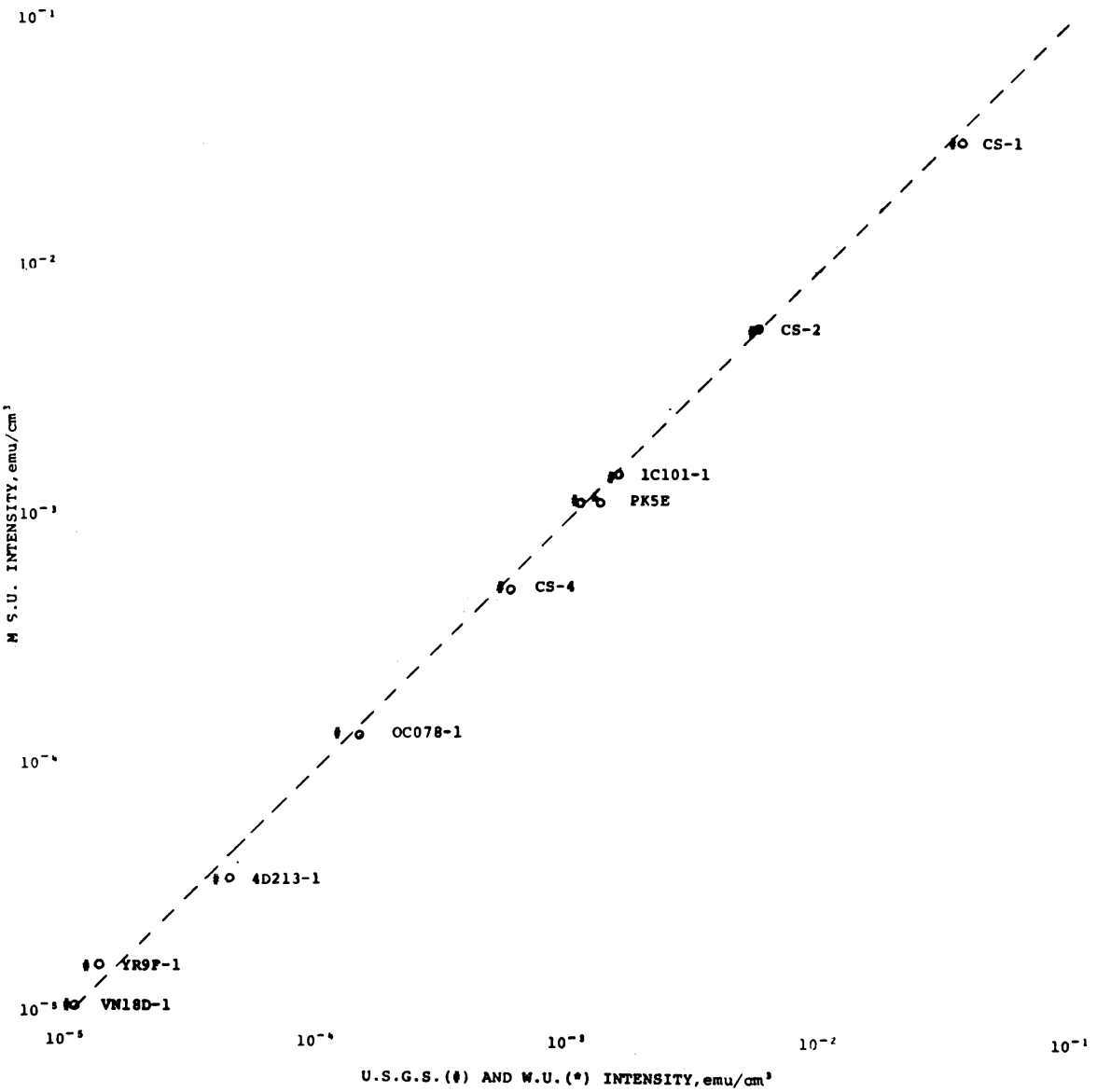

Figure 17. Intensity comparisons.

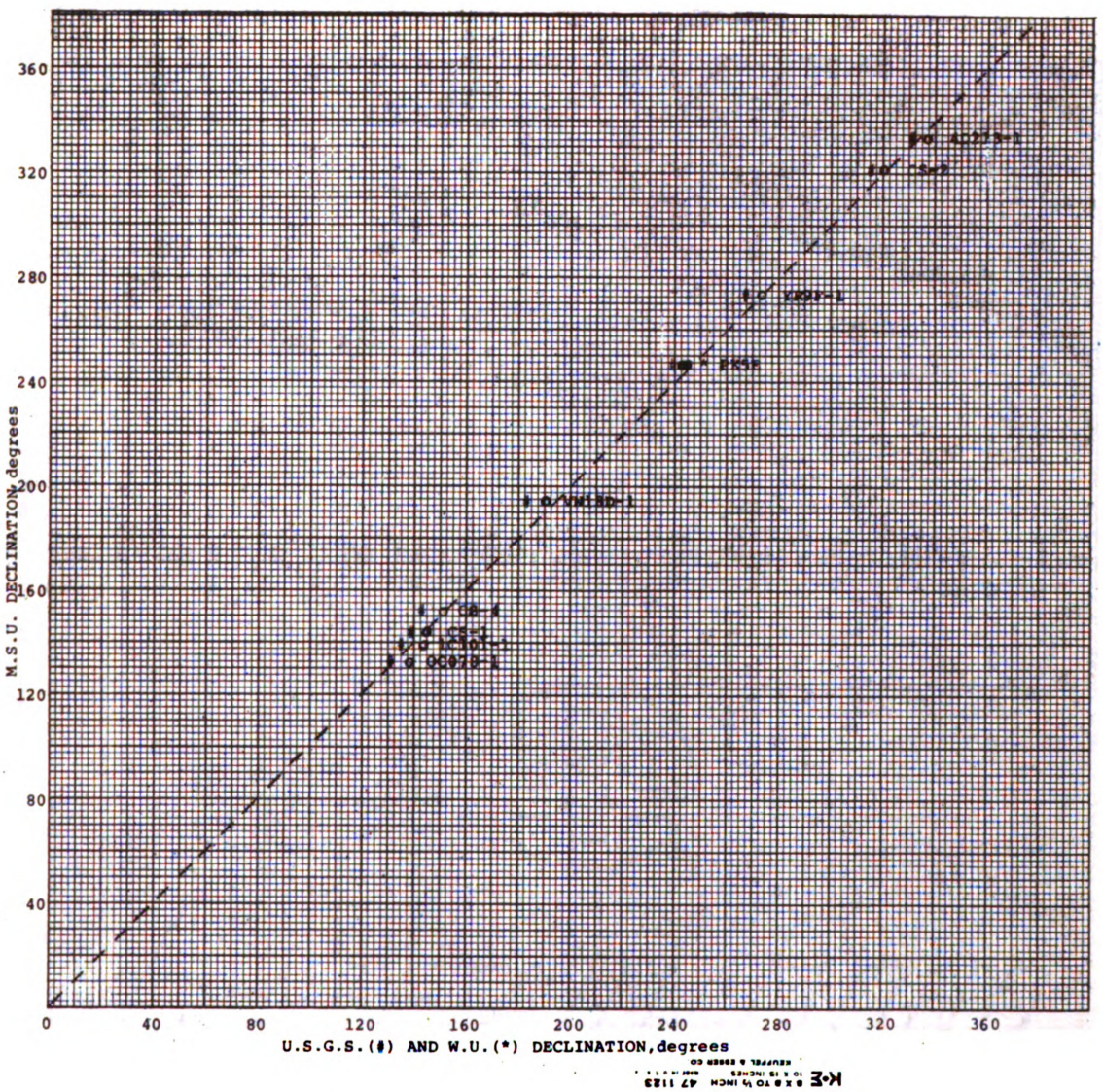

Figure 18. Declination comparisons.

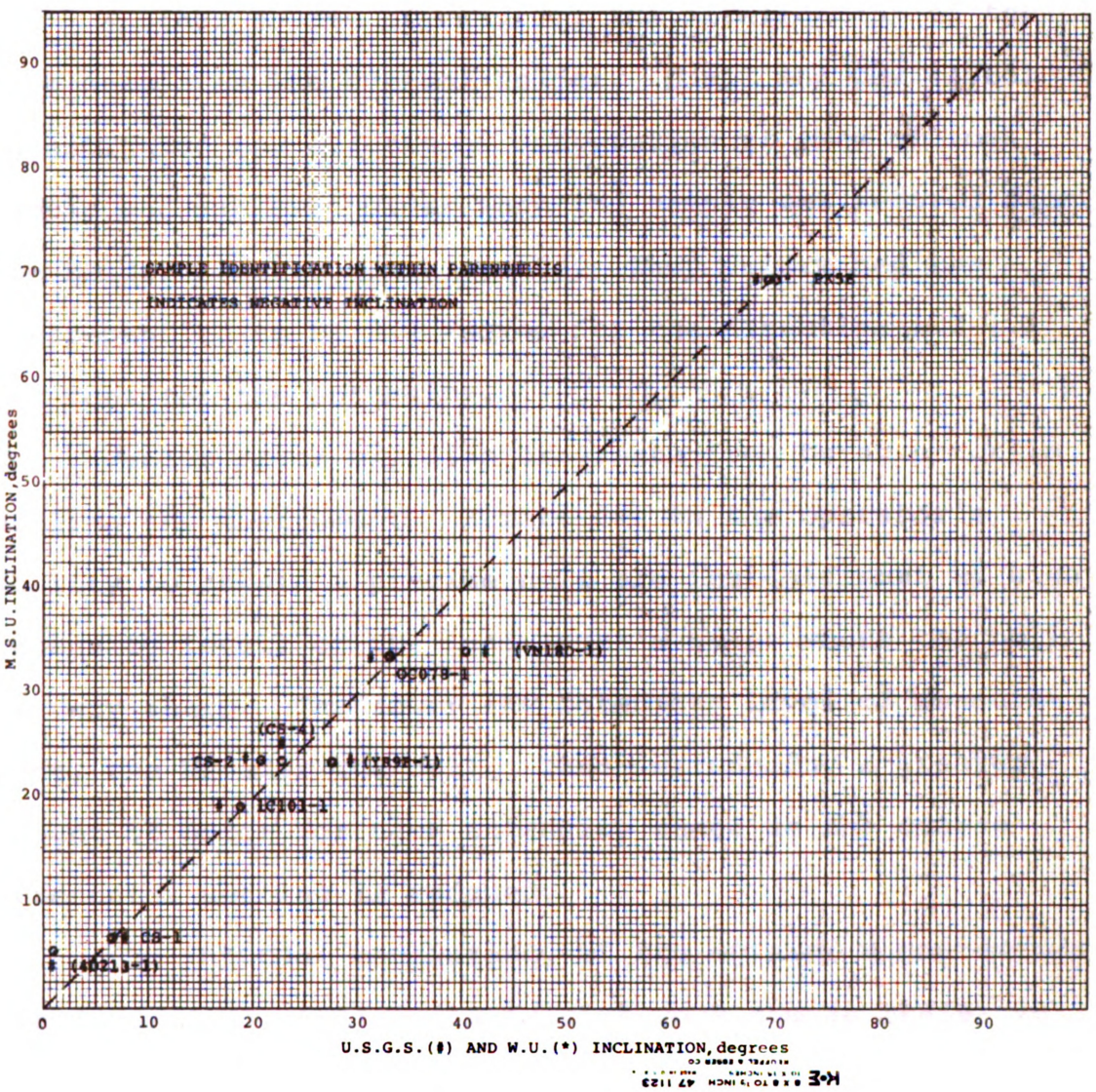

Figure 19. Inclination comparisons.

for OC078-1, 1C101-1, and 4D213-1 were respectively 0.01×10^{-3}, 0.01×10^{-4}, and 0.08×10^{-5} emu/cm^3. The maximum declination and inclination changes were 3.3 and 4.4 degrees respectively. The time lapse between these measurements was 18 months.

Another source of error is the misalignment of the rock sample in the cubical holder. Doell and Cox (1965) investigated the effects of correlation of axes of rock sample and cubical holder when the sample was removed from the holder between measurements. They determined the discrepancies to be 0.7 degree for the direction and 1.1 per cent for the intensity.

Random error may also originate from human error in nulling the instrument. Errors due to the operator's ability to obtain a precise null are insignificant at high intensity levels of the instrument's range where the null is very sharp. The lower the intensity level of measurement, the broader the null. Thus introducing a greater amount of error for each intensity range as the coarse attenuator setting is reduced.

The internal consistency of the spinner magnetometer was determined utilizing a felsite rock sample (PK5E) in which hematite is the principal magnetic material. This highly magnetically stable sample has a remanent magnetic intensity of approximately 1.17×10^{-3} emu/cm^3. The volume of the sample is 11.36 cm^3. Fifteen measurements were taken over a four-day time span without removing the

sample from the cubical holder between successive measurements. The mean value of the magnetic moment perpendicular to the +Z axis was determined to be 0.437×10^{-2} emu and the phase angle was 245.25 degrees. The small sample standard deviation of the intensity determination was 0.008×10^{-2} emu and 0.58 degree for the phase angle. The standard error of the means were determined respectively for the intensity and phase angle to be 0.002×10^{-2} emu and 0.15 degree. The percentage of error of the standard deviation to the mean in relative form for the intensity is 1.87 per cent and for the phase angle is 0.24 per cent. These calculations were based on the measurement data shown in Tables 3 and 4, respectively.

TABLE 3.--Intensity measurement data for +Z axis.

Number of Measurement	Intensity x_i x 10^{-2} emu	Deviation $(x_i - \bar{X})$ x 10^{-2} emu	Square of Deviation $(x_i - \bar{X})^2$ x 10^{-2} emu
1	0.44	+0.003	0.000009
2	0.43	-0.007	0.000049
3	0.42	-0.017	0.000289
4	0.44	+0.003	0.000009
5	0.44	+0.003	0.000009
6	0.44	+0.003	0.000009
7	0.45	+0.013	0.000169
8	0.44	+0.003	0.000009
9	0.44	+0.003	0.000009
10	0.44	+0.003	0.000009
11	0.44	+0.003	0.000009
12	0.44	+0.003	0.000009
13	0.43	-0.007	0.000049
14	0.42	-0.017	0.000289
15	0.44	+0.003	0.000009
n = 15	Σ = 6.55		Σ = 0.000935

TABLE 4.--Phase angle measurement data for +Z axis.

Number Measurement	Phase Angle x_i in degrees	Deviation $(x_i - \bar{X})$ in degrees	Square of Deviation $(x_i - \bar{X})^2$
1	245.9	+0.65	0.4225
2	245.1	-0.15	0.0225
3	244.5	-0.75	0.5625
4	245.6	+0.35	0.1225
5	245.8	+0.55	0.3025
6	245.9	+0.65	0.4225
7	244.4	-0.85	0.7225
8	245.2	-0.05	0.0025
9	245.8	+0.55	0.3025
10	245.7	+0.45	0.2025
11	245.2	-0.05	0.0025
12	245.7	+0.45	0.2025
13	244.4	-0.85	0.7225
14	244.4	-0.85	0.7225
15	245.2	-0.05	0.0025
n = 15	Σ = 3678.8		Σ = 4.7375

CHAPTER VI

OPERATIONAL PROCEDURE FOR MAGNETOMETER

The operating procedure of the spinner magnetometer is outlined below in step-wise sequence.

1. Check adjustment of clearance between the spinner head mounted on the spinner shaft and the top surface of the pick-up coil. This clearance must be set to 0.014 inch to maintain calibration of the instrument. This is accomplished by use of a feeler gauge and adjusting the control knob on the elevating pick-up coil stage to provide the proper clearance, see Figure 14.
2. Turn "on" the drive motor switch, see Figure 11.
3. Turn "on" brake-clutch and band-pass filter power supplies, see Figure 20. Adjust clutch and brake voltage only when necessary, for proper accelerations on starting and stopping of spinner shaft. It is a compromise between too rapid an acceleration, to prevent damage to sample holder and spinner head, and efficiency. CAUTION: DO NOT INCREASE CLUTCH VOLTAGE OR BRAKE

Figure 20. Brake-clutch and band-pass filter power supply.

VOLTAGE ABOVE 90 VOLTS AS INDICATED ON RESPECTIVE VOLTMETERS.

4. Turn "on" oscilloscope, see Figure 21.
5. Turn "on" General Radio, type 1232-A, tuned amplifier, and null detector (high-gain amplifier) mounted in control console, see Figures 22 and 23.
6. Insert sample to be measured in cubical sample holder so that the short lines drawn perpendicular to the index line on the prepared sample extend from the index line toward the +Y axis, which is marked on the sample holder (directed from the index line to the observer's right, when placed in the lower half of the holder). Rotate the sample in the holder and align the index line on the rock sample to coincide with the +Z axis line marked on the cubical sample holder. Place upper half of sample holder over sample and align so +Z axis line on this half coincides with that on bottom half and rock sample. Check index line alignment with +Z axis on holder. Hold securely and insert and tighten 4-40 nylon machine screws with nonferrous (brass) 1/4" diameter tightening tool. CAUTION: DO NOT OVER-TIGHTEN. SCREWS SHOULD BE TIGHTENED ONLY SNUG ENOUGH TO SECURE THE TWO SAMPLE HALVES TOGETHER SO THAT NO AIR GAP EXISTS BETWEEN THE SURFACES. If this cannot

Figure 21. Operating table, oscilloscope and control console.

Figure 22. High-gain amplifier and null detector.

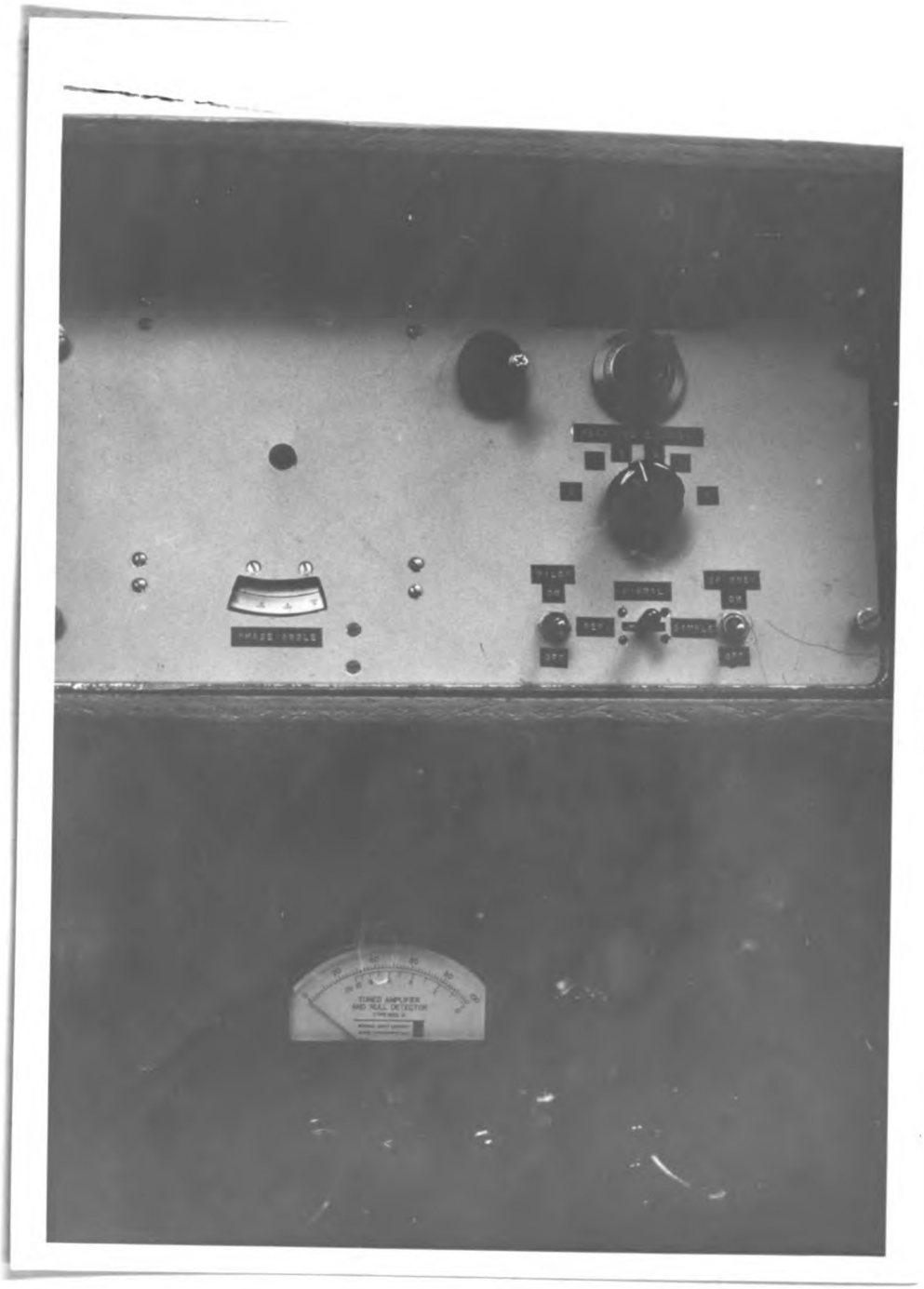

Figure 23. Control console.

be accomplished easily without having to over-tighten nylon screws, the sample is too long and should be dressed off at one end to proper over-all length, given in Table 1. CAUTION: AFTER THE SAMPLE IS PLACED IN THE CUBICAL SAMPLE HOLDER AND BEFORE TIGHTENING THE NYLON SCREWS, HOLD THE TWO HALVES SECURELY TOGETHER AND SHAKE--IF A RATTLE IS HEARD, OR IF SAMPLE INDEX LINE BECOMES MIS-ALIGNED FROM +Z AXIS LINE ON HOLDER, SAMPLE IS UNDERSIZED. In this case determine if diameter is undersize. If so, transparent tape (Scotch Magic) may be applied around center of rock sample to obtain proper fit in holder to prevent rotation in holder. Only apply enough tape to keep sample from rotating in holder. If sample is too short (and/or undersize in diameter) place a paper shim between top half of holder and rock sample, to keep it from moving or rotating within holder when shaken, or when rotated in spinner magnetometer. If the sample turns independently in the holder it cannot be accurately measured.

7. Enter sample identification, date, and observer's initials on a blank pre-printed data card, see Figure 24.
8. Insert cubical sample holder containing sample to be measured in magnetometer spinner head,

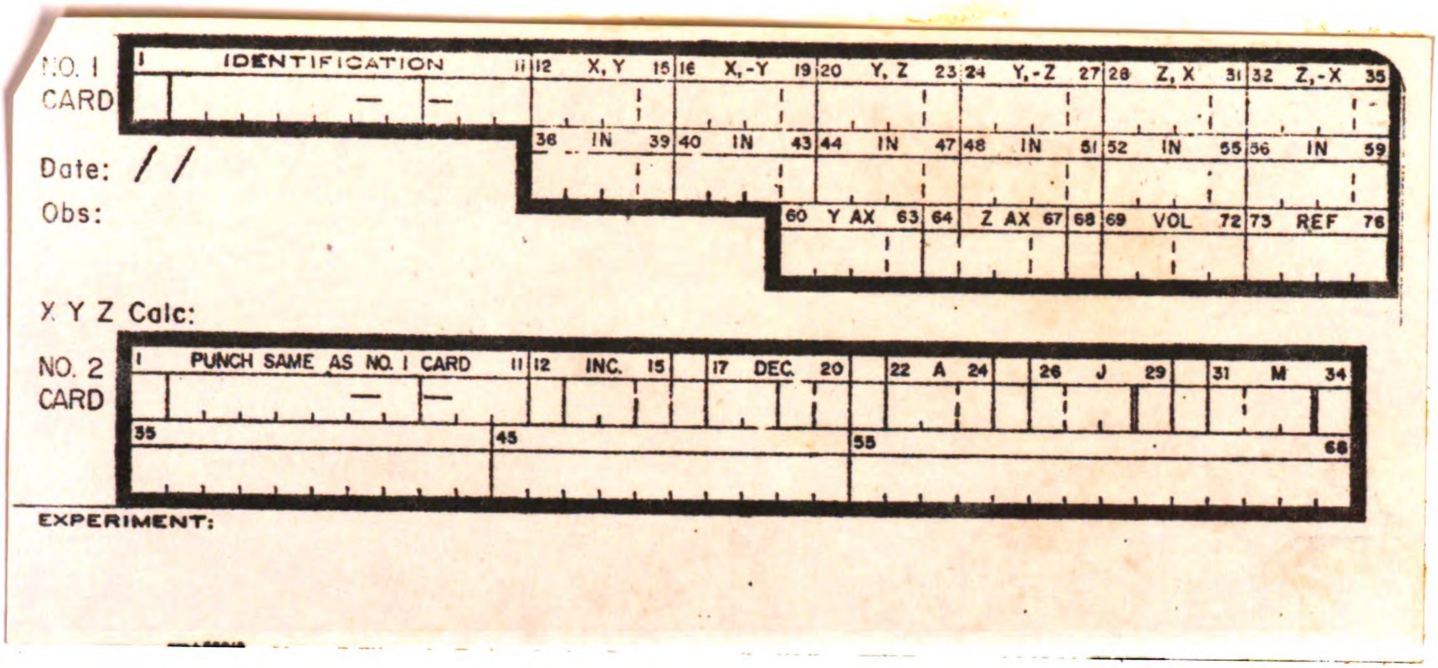

Figure 24. Data card.

see Figure 25. CAUTION: ALIGN INDEX FOR THE AXIAL DIRECTION TO BE MEASURED WITH THE INDEX ON THE SPINNER HEAD TO ASSURE MEASUREMENT OF PROPER AXIS AND DIRECTION. FOR EXAMPLE, IF IT IS DESIRED TO MEASURE THE +X AXIS, PLACE THE CUBICAL HOLDER IN THE SPINNER HEAD SO THAT +X ARROW ON THE CUBICAL HOLDER POINTS INTO THE SPINNER HEAD AND COINCIDES WITH THE INDEX ON THE SPINNER HEAD.

9. Set the Signal Switch (S1) on the mixer unit to the neutral (center) position to observe the combined reference generator and pick-up coil signals, see Figure 26. The other two positions of this switch permit independent observation of the pick-up coil signal in the "sample" (right hand) position and the reference generator signal in the REF (left hand) position.
10. Turn "on" the pilot light. This light illuminates the phase angle dial, see Figure 26.
11. Place the left hand on the gain control of the high-gain amplifier, turn "on" the "Spinner" switch with the right hand and reduce setting of gain on high-gain amplifier, to keep indicator pointer of meter on scale, see Figure 22. Turn the Spinner "off." CAUTION: OCCASIONALLY THE FILTER TUNING CONTROL ON THE HIGH-GAIN AMPLIFIER SHOULD BE TUNED FOR MAXIMUM SIGNAL INDICATION OF THE METER. IT MAY BE NECESSARY TO

Figure 25. Cubical sample holder in spinner head.

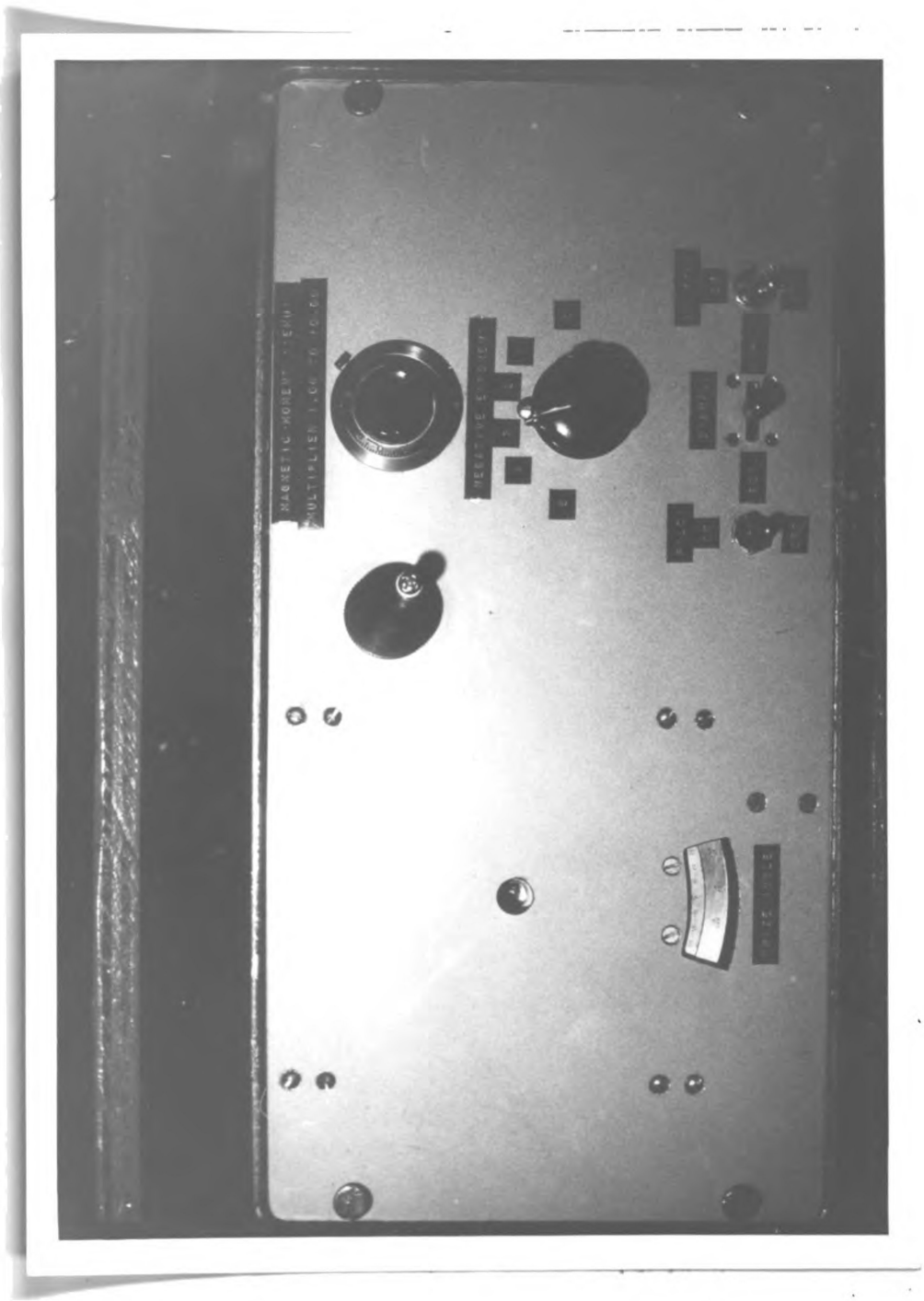

Figure 26. Phase shifter, attenuator, and mixer unit.

REDUCE THE GAIN CONTROL TO MAINTAIN THE INDICATOR POINTER ON SCALE. THE FILTER TUNING CONTROL SHOULD BE CAREFULLY TUNED TO PEAK ON THE METER. THIS ADJUSTMENT IS CRITICAL SINCE THE CIRCUIT IS HIGHLY SELECTIVE. IT SHOULD PEAK AT 100 CPS. THIS ADJUSTMENT NEED NOT BE REPEATED AS LONG AS THE INSTRUMENT IS NOT DISTURBED, OR THE FILTER TUNING CONTROL ON THE HIGH-GAIN AMPLIFIER HAS NOT BEEN CHANGED.

12. Initially it will be found that the phase angle control (crank knob) and the attenuator coarse ("T" pad, 5 step, 20 db per step potentiometer) and fine (linear 10 turn potentiometer) controls interact. The operator must acquire the feel of the instrument before readings can be made rapidly and precisely. A little practice will develop confidence in the operator. Set the following controls at mid-range: Phase angle at 180 degrees, coarse attenuator at 10^{-2} and fine attenuator at 5.00. With the left hand on the high-gain amplifier gain control, turn "on" the spinner with the right hand and maintain the meter pointer on scale by adjusting the gain with the left hand to "ride the gain" as the right hand seeks the null position by rotation of the phase angle, coarse and fine attenuator controls.

13. Turn "on" the Spinner. Observe the meter on the high-gain amplifier. Set the gain control for about 3/4 scale reading, with the left hand. Rotate the phase angle control with the right hand and note if meter level increases. If it does, reverse the direction of rotation of the phase angle control and continue to turn it until the meter indicates a minimum other than zero, which cannot be reduced with further adjustment of the control. If the meter level decreases during the initial rotation of the phase angle control, continue to turn it in the same direction until a minimum is indicated on the meter. It may be necessary to increase the setting of the gain to prevent the meter from falling to zero as the phase angle control is rotated. The object is to obtain a minimum on the meter, which indicates that the null is being approached. Any adjustment of the phase angle, coarse or fine attenuator controls that produces a reduction in meter reading indicates that the control is being adjusted in a favorable direction to achieve a null. Any increase in meter level brought about by an adjustment of any of the above controls indicates a departure from the null and the adjustment should be reversed. Once a minimum has been obtained

on the meter by adjustment of the phase angle control, adjust the fine attenuator with the right hand by rotating it in a direction which produces a reduction in meter reading. Ride the gain with the left hand to prevent the meter from going off the high end of the scale. It may be necessary to increase the gain if the meter begins to fall toward the zero end of the scale. Adjust the coarse attenuator one step, one way or the other, depending upon the end on which the fine control is set. Adjust the coarse attenuator, if necessary, and readjust the fine attenuator to indicate a decrease in meter reading. Continue rotating the fine attenuator until a minimum is obtained on the meter. Now alternately, slowly rotate the phase angle control and the fine attenuator control to obtain decreasing meter readings with each adjustment, while maintaining a measurable reading on the meter (1/3 to 1/2 scale) by riding the gain with the left hand. Once a minimum has been obtained on the meter, use the oscilloscope to obtain a null by further adjustment of the phase angle and fine attenuator controls. As the adjustment of the controls is continued, raise the gain to give a readable indication on the oscilloscope until the null is attained. The null is attained when zero

signal is indicated on the oscilloscope. This will be either a straight horizontal line or an ambient noise level sine wave pattern. The latter may be confirmed by switching the Spinner "off" and observing the noise signal on the oscilloscope without making changes in settings. The sine wave pattern should not change appreciably in form or size from the pattern observed at the null with the Spinner switched "on."

14. When the null has been attained, switch the Spinner "off." Carefully read the setting of the phase angle dial and enter its reading to the nearest 1/10 degree on the data card for the appropriate axis. Carefully read the fine attenuator setting from its dial and enter the three digits on the data card for the appropriate axis and add the negative exponent read from the coarse attenuator setting to the space on the data card provided after the fine attenuator reading.

15. Remove the cubical sample holder from the spinner head and note which axis and axial direction was measured. Place the cubical sample holder back in the spinner head so that the same axis is oppositely directed toward the spinner head and its arrow coincides with the index on the spinner head.

16. Repeat steps 13 and 14 for measurement and recording of the readings for this axial direction.

17. Repeat this operation for the + and - directions of the other two axes.

We now have + and - readings for the X, Y, and Z axes of this sample. This completes the measurement operation.

CHAPTER VII

CALCULATION OF DIRECTION AND INTENSITY OF THE REMANENT VECTOR

The direction and intensity of the remanent magnetic vector of the rock sample in situ can be determined by a numerical-graphical technique utilizing the equal area stereonet or by a numerical-trigonometric technique. The numerical-trigonometric technique lends itself to digital computer calculation and a program for the calculation is given by Doell and Cox (1965).

The numerical-graphical technique will be discussed below:

When the rock sample is obtained in the field, the plunge of the axis of sample, which is the +Z axis, is measured and the azimuth of the +Y axis is measured from true north. The Y axis is the intersection of the transverse plane of the core and a horizontal plane. The +Y axis is to the right of the observer, facing along the +Z axis. The +X axis is mutually perpendicular to the Z and Y axes and is directed upward.

The total magnetic moment of the sample according to Doell and Cox (1965) is:

$$M = \left[(M_z^2 + M_x^2 + M_y^2)/2\right]^{\frac{1}{2}} \tag{1}$$

$$M \simeq \tfrac{1}{2}\,(M_{z_1}^2 + M_{z_2}^2 + M_{x_1}^2 + M_{x_2}^2 + M_{y_1}^2 + M_{y_2}^2)^{\frac{1}{2}}. \tag{2}$$

The magnetic components of the rock sample are shown in Figure 27.

The magnetic intensity of the sample is determined by dividing its total moment by the sample volume.

The identification of the magnetometer observations is tabulated in Table 5.

The first step in determining the direction of the remanent magnetic vector is to average the positive and negative spins for each axis, where the subscripts 1 and 2 represent the positive and negative spins respectively:

$$\begin{aligned} \phi_z &= \tfrac{1}{2}(360^0 + \phi_{z_1} - \phi_{z_2}) \\ \phi_x &= \tfrac{1}{2}(360^0 + \phi_{x_1} - \phi_{x_2}) \\ \phi y &= \tfrac{1}{2}(360^0 + \phi_{y_1} - \phi_{y_2}) \end{aligned} \tag{3}$$

The next step is to determine the direction of the vector with respect to the axes of the rock sample, using the stereonet as illustrated in Figure 28. This is accomplished by determining the intersection of the three great circles representing ϕ_z, ϕ_x, and ϕ_y.

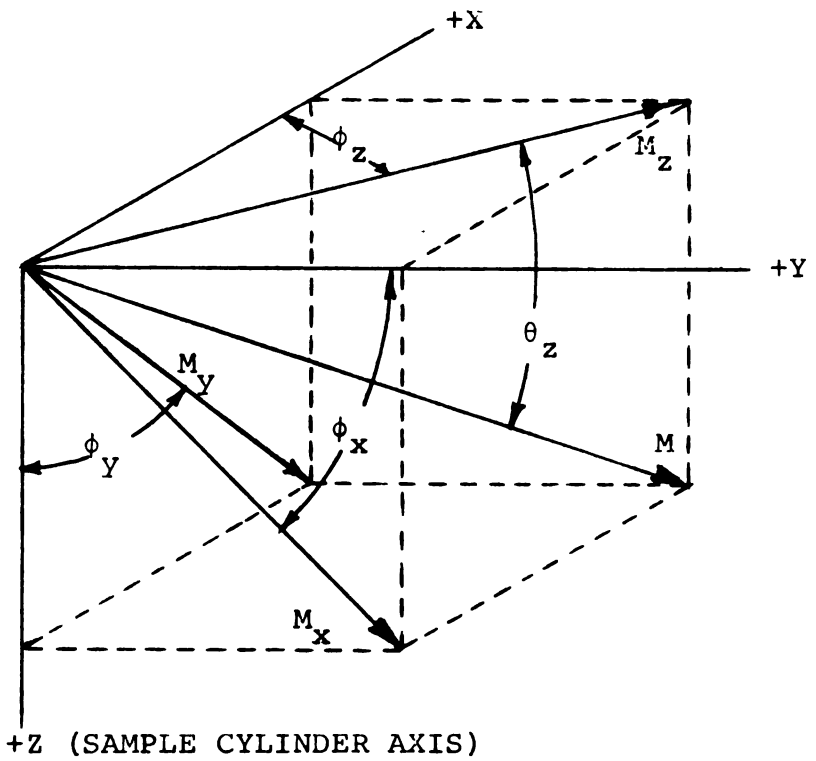

Figure 27. Identification of rock sample magnetic components.

TABLE 5.--Identification of magnetometer observations.

Component Measured		Axis Directed Into Spinner Shaft	Axis Directed Toward Index on Spinner Head	Axis Directed 90° Clockwise of Index	Spin Reference
Phase Angle	Moment				
ϕ_{z_1}	M_{z_1}	+z	+x	+y	1
ϕ_{z_2}	M_{z_2}	-z	+x	-y	2
ϕ_{x_1}	M_{x_1}	+x	+y	+z	3
ϕ_{x_2}	M_{x_2}	-x	+y	-z	4
ϕ_{y_1}	M_{y_1}	+y	+z	+x	5
ϕ_{y_2}	M_{y_2}	-y	+z	-x	6

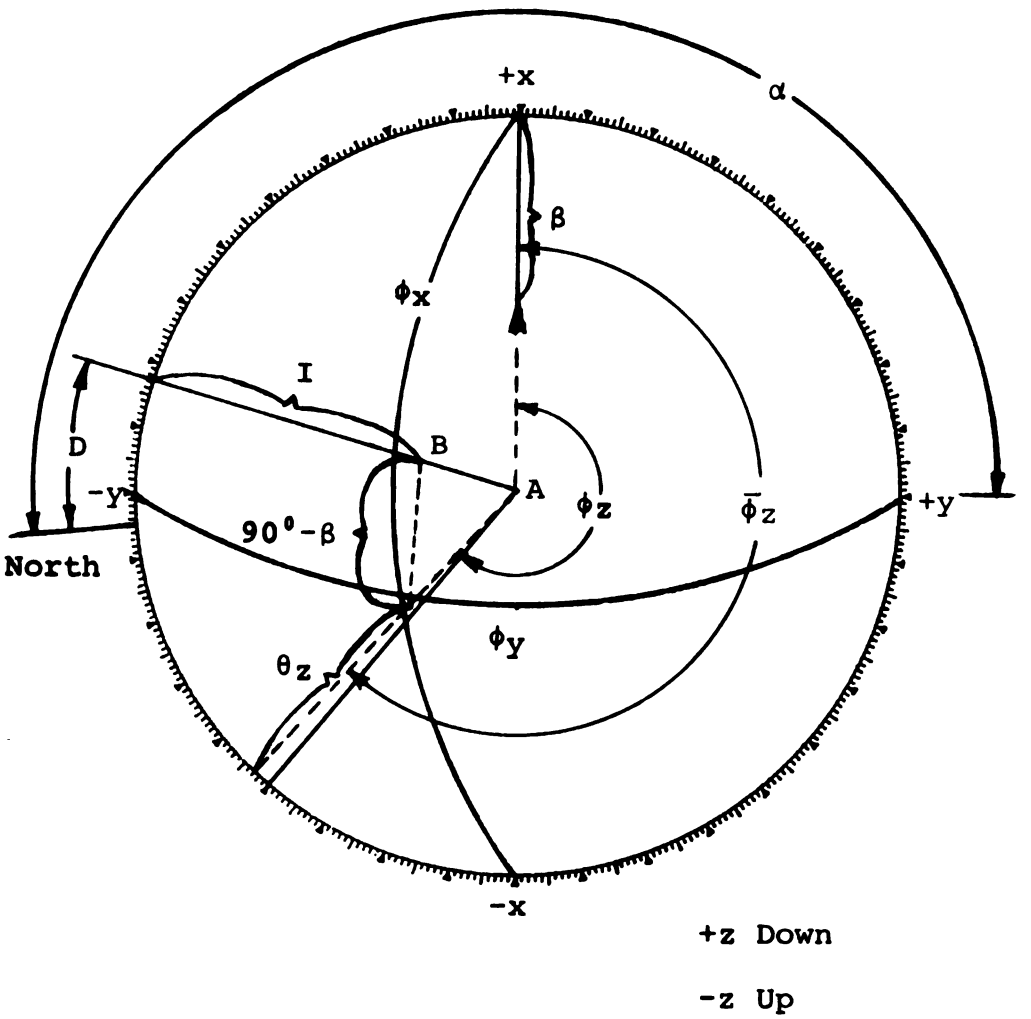

Figure 28. Graphical stereographic direction determinations.

By convention:

ϕ_z is measured from +X to +Y

ϕ_x is measured from +Y to +Z

ϕ_y is measured from +Z to +X.

In practice, these planes normally do not have a common intersection point, but define a triangle. The circle inscribed in the triangle defines the error of the solution and a line drawn from the center of the stereonet through the center of the circle to the perimeter represents the plane of the magnetic vector with respect to the axial system. The azimuth of this line taken with respect to the +X axis is designated as the magnetic vector $\overline{\phi}_z$. The inclination θ_z of the magnetic vector is the angle represented by the distance between the perimeter and the center of the circle along the line drawn through the center of the stereonet.

To determine the position of this magnetic vector in situ, the following procedure is used. The plunge β of the Z axis of the sample is measured inward from the perimeter along the +X axis and a vector is drawn from the center of the stereonet to this point representing the position of the Z axis. Using a dashed line, if below the horizon or a solid line, if above. The +Z axis of the sample is rotated through an angle of (90-β) degrees in the direction of the +X axis. The magnetic vector is also rotated an angle of (90-β) degrees along a small circle about the Y

axis, as shown in Figure 28. The in situ magnetic vector is now represented by the line A-B. The inclination I of the magnetic vector is measured inward from the perimeter along the projection of the line A-B.

The magnetic north azimuth α measured in the field is laid off in a counterclockwise direction with respect to the horizontal +Y axis.

The declination D of the magnetic vector is then read in a clockwise direction from magnetic north to the line representing the in situ direction of the magnetic vector.

CHAPTER VIII

RESULTS OF SAMPLE MEASUREMENTS

The remanent magnetization of a suite of 57 rock samples collected from nine sites within the Melrose stock were investigated.

The Melrose stock is located in the Dolly Varden mountains, 25 miles west of the eastern Nevada border in southeastern Elko County, at 40° 20' North latitude, 114° 35' West longitude, as shown in the insert in Figure 29. The stock is a Cretaceous igneous instusive mass of porphyritic quartz monzonite, approximately 12 square miles in area. It has intruded into Paleozoic limestone sediments which are metamorphosed by the intrusive. Local lava flows, pyroclastics, and alluvial deposits are also found within the area. Further information regarding the geology of the area may be found in Snow (1963).

Figure 29 is a geologic map of the Melrose stock and the immediate surrounding area after Snow (1963). This map shows the location of the sampling sites by identification numbers. Sites 2, 3, 4, 5, and 11 are located

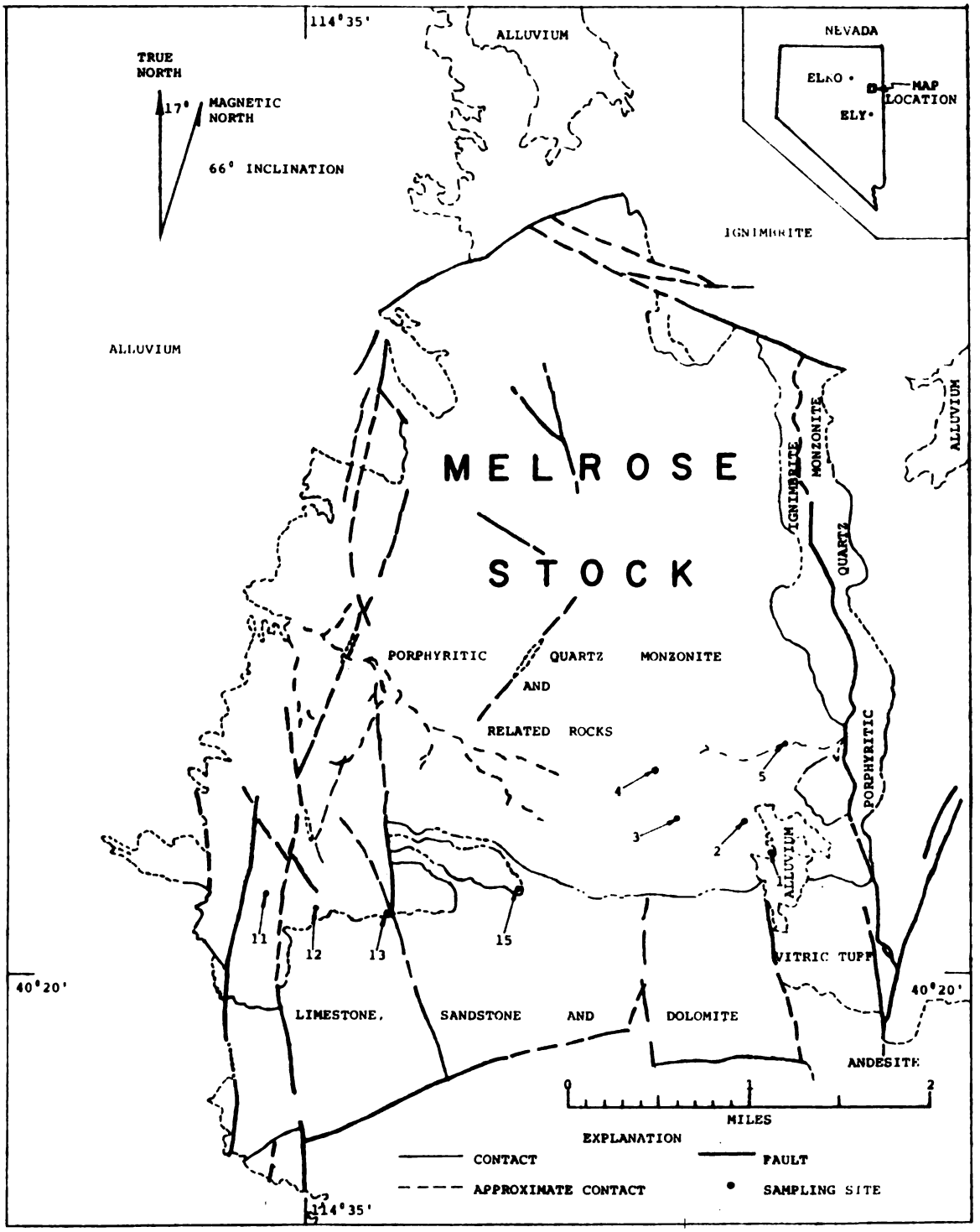

Figure 29. Geologic map of Melrose stock after G. G. Snow.

well within the intrusive, while the remainder are located near the margin of the intrusive, as mapped by Snow (1963). An average of six oriented core samples were taken per site. Each sample collected in the field measured one-inch in diameter and approximately two and one-half inches in length.

The mineral percentage composition of the Melrose stock porphyritic quartz monzonite for selected samples as determined by thin section petrology by Mr. Dewey Sanderson are tabulated in Table 6.

Table 7 is a tabulation of NRM measurements of samples taken from the nine sites within the Melrose stock. This table includes the date on which the measurement was taken, declination, inclination, and intensity for each sample.

Figures 30 through 38 illustrate the direction of the remanent magnetism on a series of equal area projections for each of the nine sites. The "X" on each diagram represents the direction of the earth's magnetic field in the Dolly Varden Mountain area. NRM vectors above the horizon are indicated by the symbol "o" and those below by the symbol ".". Individual samples are identified by assigned letter within each site. Examination of the equal area projections of the various sites indicate a significant amount of dispersion in the NRM directions of the samples. The data on which the figures and tables included in the paper are based, were obtained from NRM

TABLE 6.--Mineral composition of Melrose stock porphyritic quartz monzonite.

Sample	Volume Percentage of Mineral Content					
	Plagio-clase	Potash Feld-spar	Quartz	Horn-blend	Biotite	Magnetite
VN1A	29.6	42.5	0.6	15.6	8.6	2.7
VN2A	33.6	37.6	6.0	16.8	4.4	1.6
VN2B	37.6	36.0	7.6	14.6	2.2	2.0
VN3A	51.8	25.3	7.1	12.4	2.0	1.6
VN4E	38.8	41.2	7.0	10.2	1.8	1.4
VN5E	32.1	39.7	8.6	12.9	4.6	2.2
VN11A	38.2	28.6	22.2	3.4	7.2	0.6
VN11D	38.0	24.4	26.2	4.8	5.4	1.0
VN11E	36.6	23.4	29.4	4.0	4.4	2.2
VN11F	37.6	19.4	30.6	4.8	6.4	0.8
VN12B	45.0	18.8	26.4	2.6	7.0	0.4
VN13D (1)	36.6	26.0	29.6	3.6	3.2	1.0
VN13D (2)	39.7	24.6	25.1	5.1	3.4	2.2
VN15C	14.3	70.7	7.7	6.1	1.0	0.4
Average %	36.4	32.7	16.7	8.4	4.4	1.4

Total Percentage = 100.0

TABLE 7.--NRM measurements of samples.

Sample	Date	Declination (Degrees)	Inclination (Degrees)	Intensity x $10^{-(\ )}$ (emu/cm^3)
VN1A	2-6-70	49.0	39.9	4.05 - (4)
VN1B	2-6-70	12.8	41.5	5.15 - (4)
VN1C	2-6-70	69.9	61.7	5.48 - (4)
VN1D	2-12-70	288.1	17.1	5.13 - (4)
VN1E	2-6-70	158.0	26.3	3.15 - (3)
VN1F	2-6-70	247.9	-30.0	1.45 - (3)
VN2A	2-6-70	22.6	56.3	3.96 - (4)
VN2B	2-6-70	276.5	59.9	2.08 - (4)
VN2C	2-6-70	105.8	-21.5	1.41 - (3)
VN2D	2-6-70	39.5	46.4	3.98 - (4)
VN2E	2-13-70	117.9	21.6	3.96 - (4)
VN2F	2-6-70	283.6	27.7	3.63 - (2)
VN2G	2-6-70	337.7	73.8	2.12 - (4)
VN3A	2-6-70	292.3	-5.7	1.34 - (4)
VN3B	2-6-70	96.8	16.0	1.67 - (4)
VN3C	2-6-70	338.2	88.1	6.48 - (4)
VN3D	2-6-70	NO	STRONG	INTERSECTION
VN3E	2-6-70	27.6	58.2	7.65 - (4)
VN3F	2-6-70	113.8	-72.9	8.83 - (5)
VN4A	2-12-70	348.1	52.8	2.42 - (4)
VN4B	2-12-70	301.7	40.6	2.64 - (4)
VN4C	2-12-70	347.7	-15.0	1.02 - (4)
VN4D	2-12-70	131.8	88.9	2.12 - (4)
VN4E	2-12-70	0.2	55.3	3.77 - (4)
VN4F	2-12-70	28.3	83.2	2.72 - (4)
VN4G	2-12-70	285.4	-16.1	1.37 - (4)
VN5A	2-12-70	282.1	- 8.3	1.37 - (3)
VN5B	2-12-70	211.4	-61.0	1.73 - (4)
VN5C	2-12-70	242.4	80.2	2.52 - (5)
VN5D	2-12-70	333.3	50.8	4.09 - (4)
VN5E	2-12-70	266.5	20.7	3.58 - (4)
VN5F	2-12-70	18.4	-17.6	2.28 - (4)
VN11A	2-12-70	338.6	80.6	2.28 - (4)
VN11B	2-12-70	311.8	61.9	1.13 - (4)
VN11C	2-12-70	335.1	72.4	1.22 - (4)
VN11D	2-12-70	358.8	47.8	2.14 - (4)
VN11E	2-12-70	339.3	60.4	9.44 - (5)
VN11F	2-12-70	104.5	63.0	1.55 - (4)
VN12A	2-12-70	53.0	57.3	9.61 - (5)
VN12B	2-12-70	82.0	68.1	7.96 - (5)
VN12C	2-12-70	54.5	53.7	8.09 - (5)
VN12D	2-12-70	146.7	51.5	2.08 - (3)
VN12E	2-12-70	237.5	57.2	1.99 - (4)
VN13A	2-13-70	259.6	49.1	1.81 - (4)

TABLE 7--Continued.

Sample	Date	Declination (Degrees)	Inclination (Degrees)	Intensity x $10^{-(\ )}$ (emu/cm^3)
VN13B	2-13-70	343.2	40.6	2.54 - (4)
VN13C	2-13-70	249.3	39.5	2.91 - (4)
VN13D	2-13-70	230.0	44.2	2.17 - (4)
VN13E	2-13-70	171.2	55.7	2.19 - (4)
VN13F	2-13-70	351.3	-18.7	1.06 - (2)
VN15A	2-13-70	48.3	45.2	3.33 - (4)
VN15B	2-13-70	77.7	63.4	3.00 - (4)
VN15C	3-13-70	28.8	76.4	2.92 - (3)
VN15D	2-13-70	80.8	67.7	5.48 - (3)
VN15E	2-13-70	125.1	11.1	8.14 - (4)
VN15F	2-13-70	57.7	48.9	2.90 - (4)

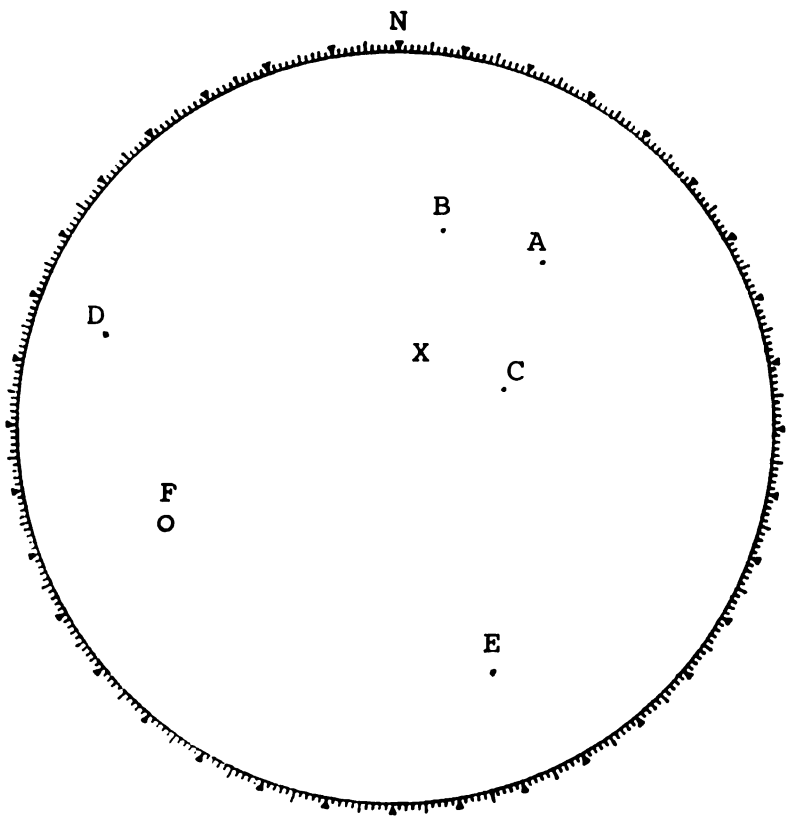

Figure 30. Equal area projection for Site VN-1 samples.

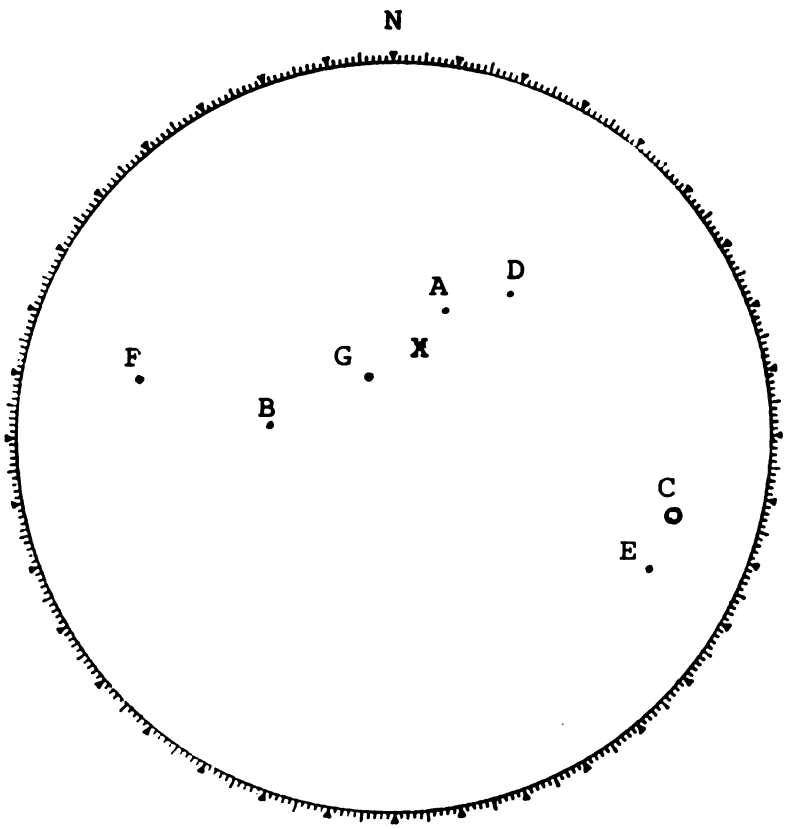

Figure 31. Equal area projection for Site VN-2 samples.

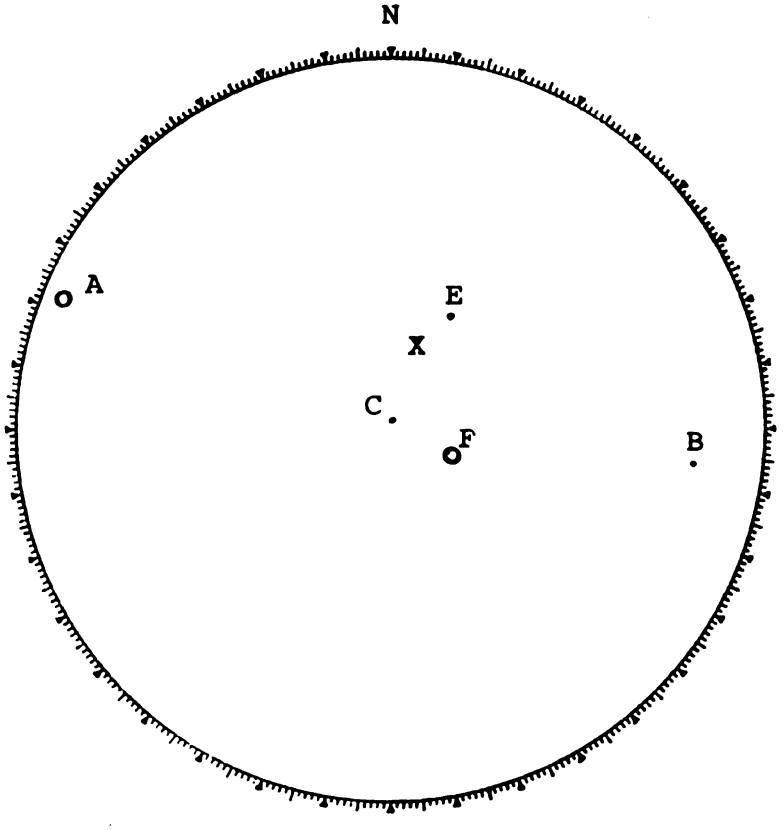

Figure 32. Equal area projection for Site VN-3 samples.

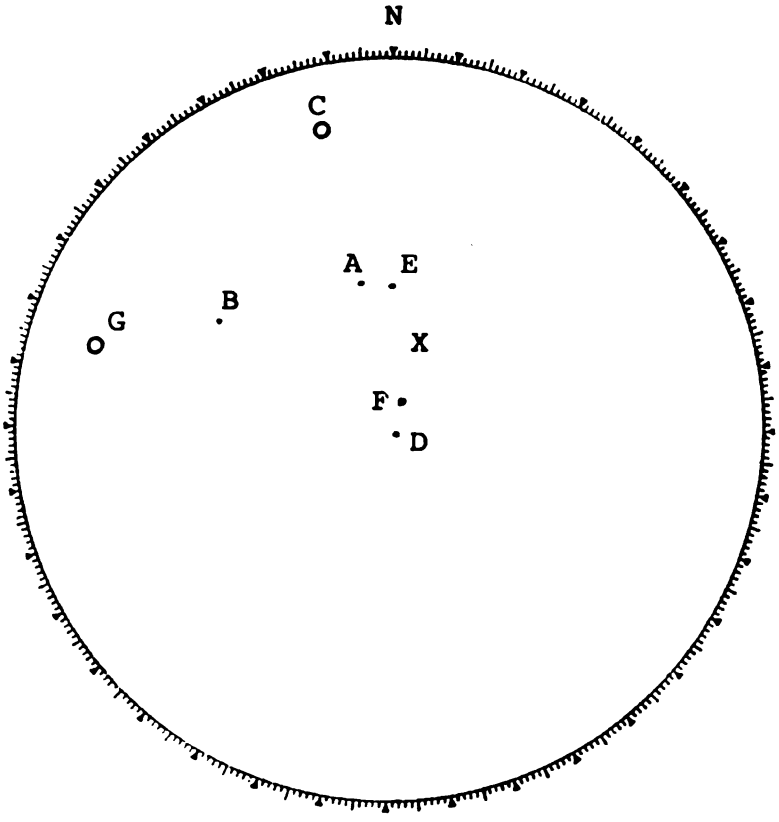

Figure 33. Equal area projection for Site VN-4 samples.

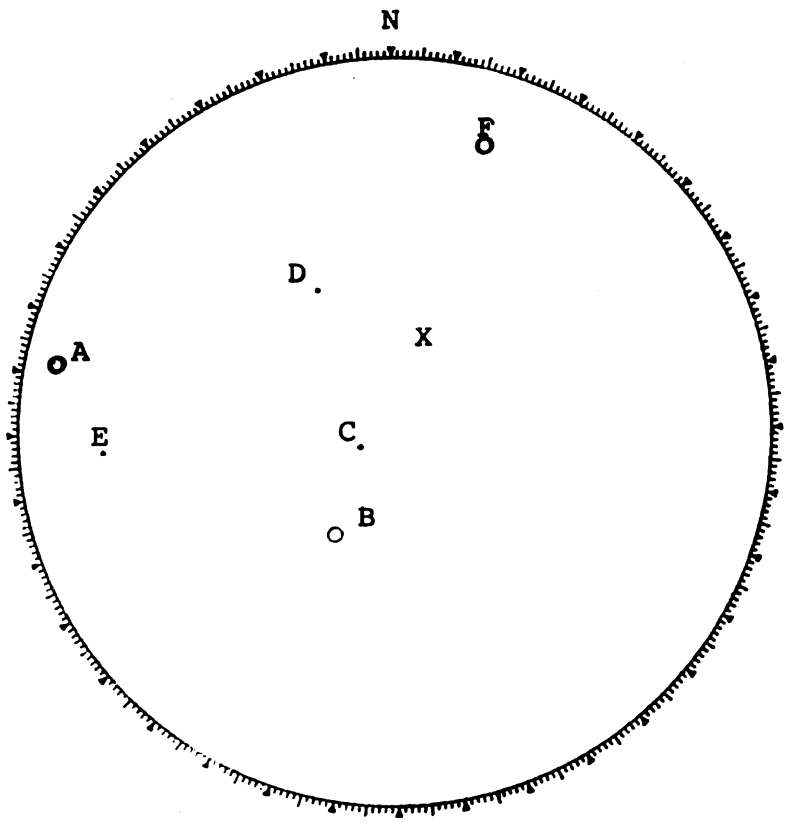

Figure 34. Equal area projection for Site VN-5 samples.

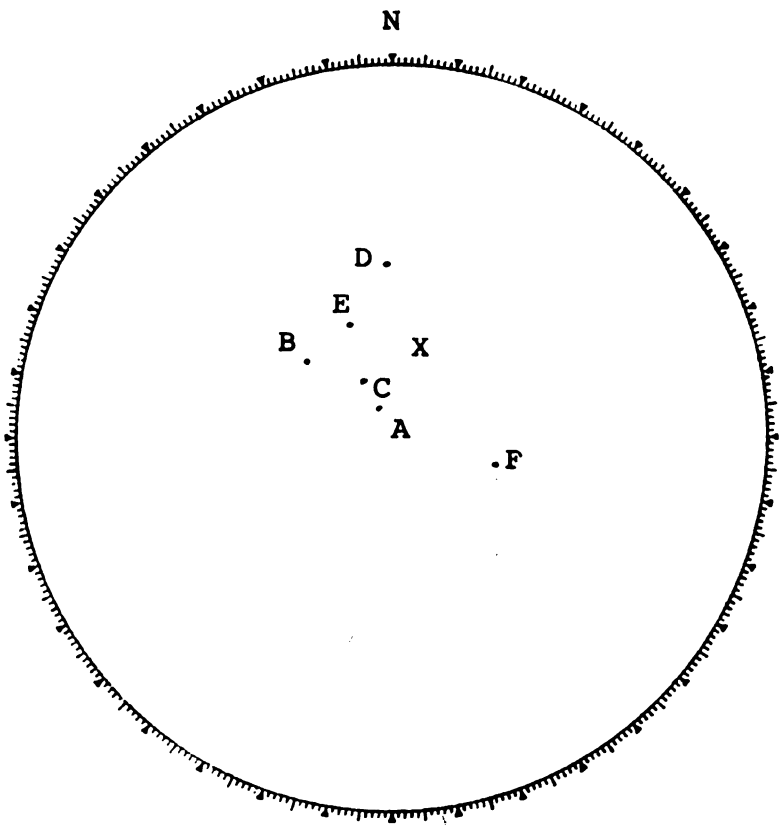

Figure 35. Equal area projection for Site VN-11 samples.

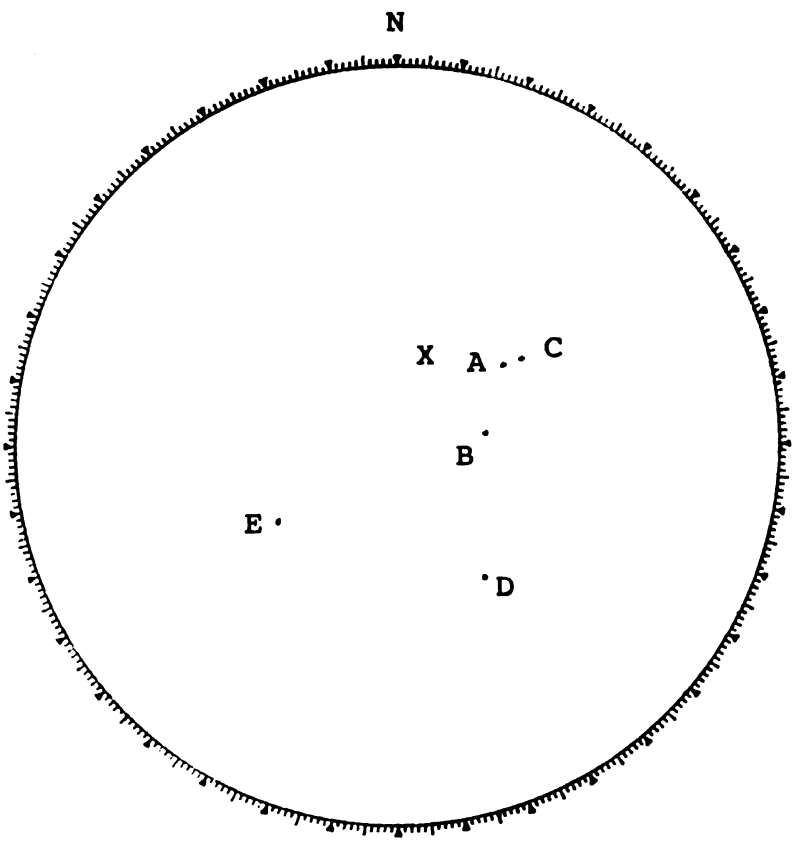

Figure 36. Equal area projection for Site VN-12 samples.

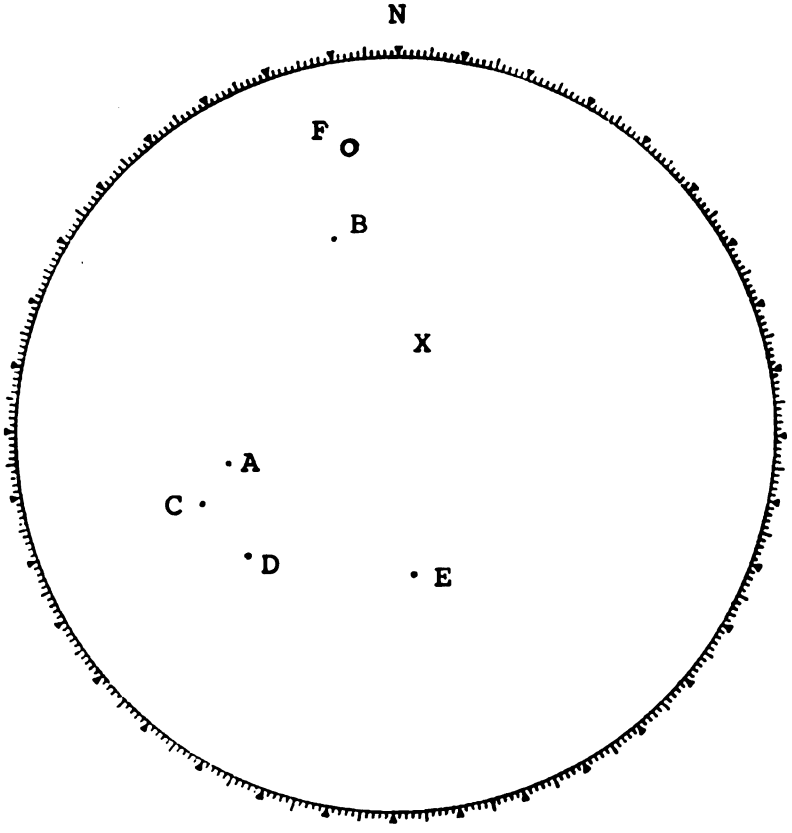

Figure 37. Equal area projection for Site VN-13 samples.

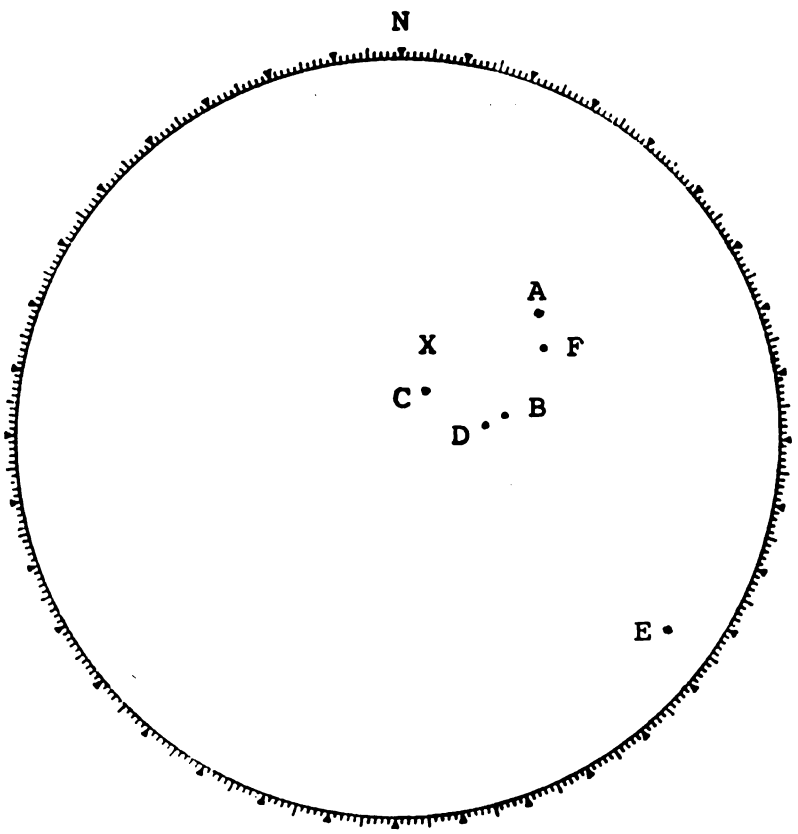

Figure 38. Equal area projection for Site VN-15 samples.

measurements made on samples as they were taken from the site. Less dispersion would possibly be obtained if the soft magnetic components were removed through appropriate magnetic cleaning techniques.

Figure 39 illustrates the average NRM intensity of selected samples from each site with respect to the distance from intrusive contact. Those samples that had an excursion factor of three or more from the mode were discarded in calculating the average. These discarded measurements were highly dispersive in direction. No correlation of NRM intensity with distance from the contact is evident. Removal of the soft magnetic component should reduce the amount of scatter and possibly produce a more distinct change in magnetic intensity in terms of distance from the intrusive contact. Furthermore, more detailed geologic study of the stock may show that the exposed surface is near the crest of the stock. If this is the case and the intrusive contact is irregular, samples from within the intrusive may lie closer to the contact than indicated on the plan map.

Table 8 is a tabulation of the Fisher distribution showing the dispersion in the directions of NRM after Irving (1964). The circle of confidence is defined in this case as a circle whose radius includes 95 per cent of the individual magnetic directions obtained from measurements within a site. These circles are centered on the true mean. The precision parameter determines the dispersion

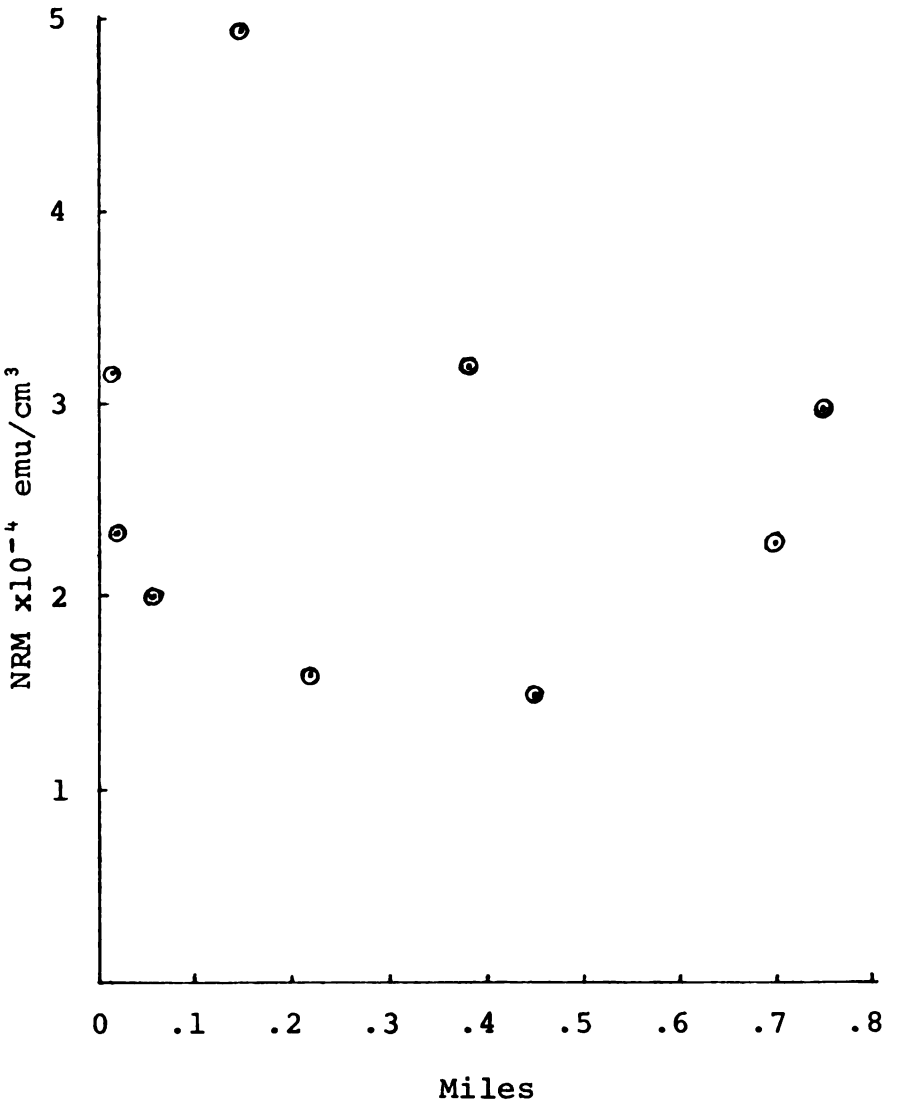

Figure 39. NRM versus distance from intrusive contact.

TABLE 8.--Fisher distribution.

Site	Number of Samples	Mean Dec. in Degrees	Mean Inc. in Degrees	Radius of Circle of Confidence (95) in Degrees	Precision Parameter
VN-1	5	344.0	55.3	101.4	1.54
VN-2	6	2.8	67.8	59.9	2.21
VN-3	4	273.6	3.2	174.7	1.39
VN-4	7	327.8	47.9	43.5	2.88
VN-5	4	260.4	14.1	106.5	1.75
VN-11	7	12.6	66.4	23.3	7.67
VN-12	5	45.2	70.3	32.1	6.63
VN-13	6	288.6	52.5	54.3	2.48
VN-15	5	81.3	50.8	31.1	7.00

of the magnetic directions. The larger the precision parameter, the closer the directions converge on the true mean. In the event the precision parameter equals zero, the directions assume a uniform random distribution. From the data given in Table 8, site VN-11 has the least dispersion of the sites studied. Site VN-3 has the greatest dispersion. The amount of dispersion compares well with the variations shown on equal area projections included in Figures 30 through 38 as expected. These circles of confidence would have been reduced in radii if the discarded samples from each site had been excluded from the Fisher distribution analysis.

The relative dispersion of the magnetic directions with respect to distance from the intrusive contact is illustrated in Figure 40.

The variability of measured and calculated parameters is summarized in tabular form in Table 9. The only generalization possible from this summary is that there are no correlations between the measured volume percentage of magnetite, intensity of NRM, precision parameter, and distance from contact.

Further geologic study of the stock based on more structural and petrologic data, and more complete sampling of the instusive, may produce results which will point out relationships not apparent in the present limited data.

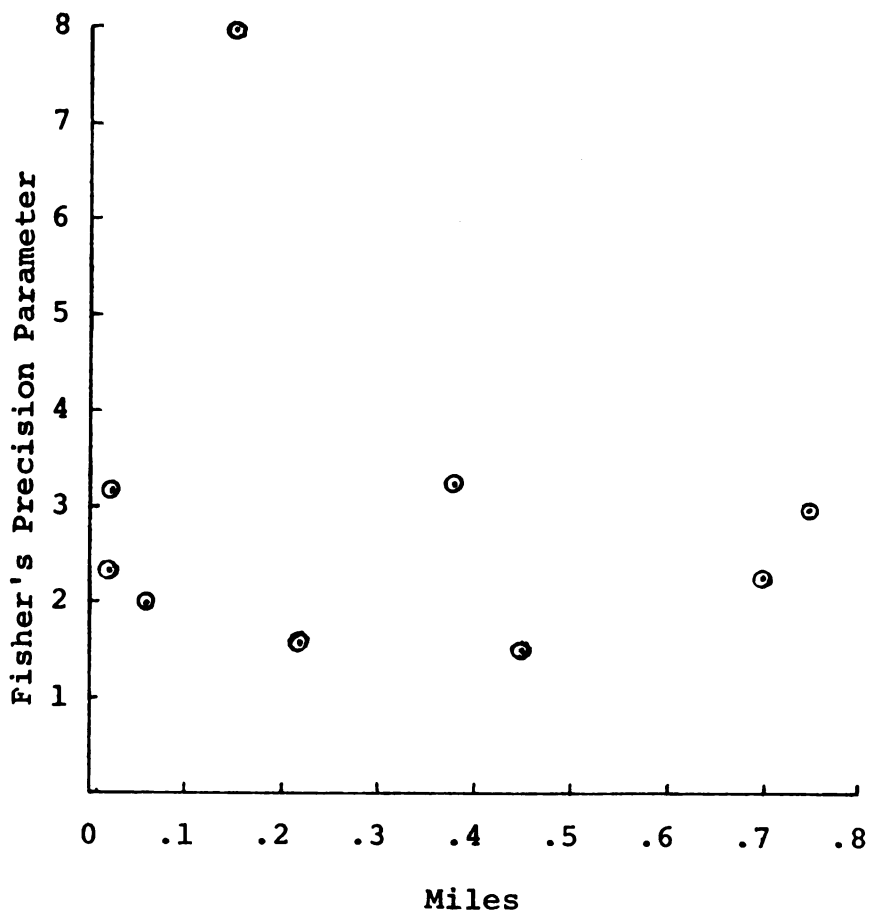

Figure 40. Dispersion versus distance from intrusive contact.

TABLE 9.--Variability from site to site.

Site	Percentage Magnetite	NRM x 10^{-4} emu/cm^3	Fisher's Precision Parameter	Distance From Contact in Miles
VN-1	2.7	4.95	1.54	0.15
VN-2	1.8	3.22	2.21	0.38
VN-3	1.6	1.50	1.39	0.45
VN-4	1.4	2.29	2.88	0.70
VN-5	2.2	2.92	1.75	0.75
VN-11	1.1	1.66	7.67	0.22
VN-12	0.4	1.99	6.63	0.06
VN-13	1.6	2.32	2.48	0.02
VN-15	0.4	3.16	7.00	0.02
Average	1.5	2.66	3.72	0.36

CHAPTER IX

SUMMARY

A spinner magnetometer has been constructed after the original design of Doell and Cox (1965). Modifications have been made in their design to increase the efficiency and versatility of the instrument.

The six spin, 12 measurement technique can be accomplished in less than six minutes. Provision has also been made for the measurement of samples over a range of diameters.

The calibration of the instrument has been checked against measurements made on samples by other laboratories. The standard deviation between these measurement determinations is 3.7 and 3.2 degrees for the declination and inclination respectively, and for the intensity, disregarding the decade unit, is 0.39 emu/cm^3.

The magnetometer is capable of measuring magnetic intensities from 1×10^{-1} to 1×10^{-6} emu/cm^3.

No correlation was found between the intensity of the NRM and the magnetite content or the distance of the samples from the edge of the Melrose stock. However, the

results are not conclusive because of limited geologic information and sampling and perhaps because the samples were not treated by magnetic cleaning techniques.

LIST OF REFERENCES

LIST OF REFERENCES

COLLINSON, D. W., CREER, K. M., and RUNCORN, S. K., 1967. Methods in Paleomagnetism, Chap. 2, Elsevier, New York, N.Y.

DOELL, R. R., and COX, A., 1965. Measurement of the Remanent Magnetization of Igneous Rocks, Geological Survey Bulletin 1203-A, U.S. Government Printing Office, Washington, D.C.

FOGEL, C. M. Introduction to Engineering Computations, Chap. 4, International, Scranton, Pa.

IRVING, E., 1964. Paleomagnetism: Its Application to Geological and Geophysical Problems, Chap. 4, Wiley, New York, N.Y.

REINTJES, J. F., and COATE, G. T., 1952. Principles of Radar, Chap. 5, McGraw-Hill, New York, N.Y.

SNOW, G. G., 1963. Mineralogy and Geology of the Dolly Varden Mountains Elko County, Nevada, Ph.D. Thesis, University of Utah.

APPENDICES

APPENDIX A

COMPONENTS FOR BRAKE-CLUTCH POWER SUPPLY

APPENDIX A

COMPONENTS FOR BRAKE-CLUTCH POWER SUPPLY

Symbol	Specifications
C1, C2	Capacitor, paper, 5 microfarad, 200 working volts direct current.
F1	Fuse, Littlefuse, type 8AG fast acting instrument, 1/2 ampere.
PL1	Neon lamp, type NE-51 1/25 watt, 65 volts, alternating current.
R1	Resistor, carbon composition, 22 ohms, 1/2 watt.
R2, R3	Potentiometer, wire wound, 1,000 ohms, 75 watts.
R4	Resistor, pilot lamp series adjust value to firing point of lamp.
RY1	Relay, double pole, double throw, 115 volts alternating current.
SR1, SR2, SR3, SR4	Rectifier, silicon, 400 volt, 2 ampere.
SW1	Switch, toggle, single pole, single throw, 10 ampere, 115 volts.
A1, A2	Ammeter, 3 ampere, direct current.
V1, V2	Voltmeter, 250 volts direct current.
TS1	Terminal strip, screw type, 12 contact.

APPENDIX B

COMPONENTS FOR 135 VOLT POWER SUPPLY

APPENDIX B

COMPONENTS FOR 135 VOLT POWER SUPPLY

Symbol	Specifications
C1, C2	Capacitor, electrolytic, 100 microfarad, 200 working volts direct current.
F1	Fuse, Littlefuse, type 8AG fast acting instrument, 1/2 ampere.
L1, L2	Filer choke, 20 henry, 50 milliampere.
PL1	Lamp, pilot, type 47, 6 volt, 0.15 ampere.
R1	Resistor, carbon composition, 1,000,000 ohms, 1/2 watt.
R2, R3	Resistor, carbon composition, 22 ohms, 1/2 watt.
R4	Resistor, wire wound 3,000 ohms, 20 watt.
R5	Resistor, wire wound with slider, 6,000 ohms, 20 watt.
SR1, SR2	Rectifier, silicon, 1,000 peak inverse volts, 0.4 ampere.
SW1	Switch, single pole single throw, 115 volts, 10 ampere.
T1	Transformer, 450 volts center tapped, 30 milliampere, 6.3 volts, 500 milliamperes.

Symbol	Specifications
VR150	Tube, gas voltage regulator type VR 150.
V1	Voltmeter, 250 volts direct current.
TS1	Terminal strip, screw type, 12 contact.

APPENDIX C

SCHEMATIC DIAGRAM OF 135 VOLT POWER SUPPLY

APPENDIX C

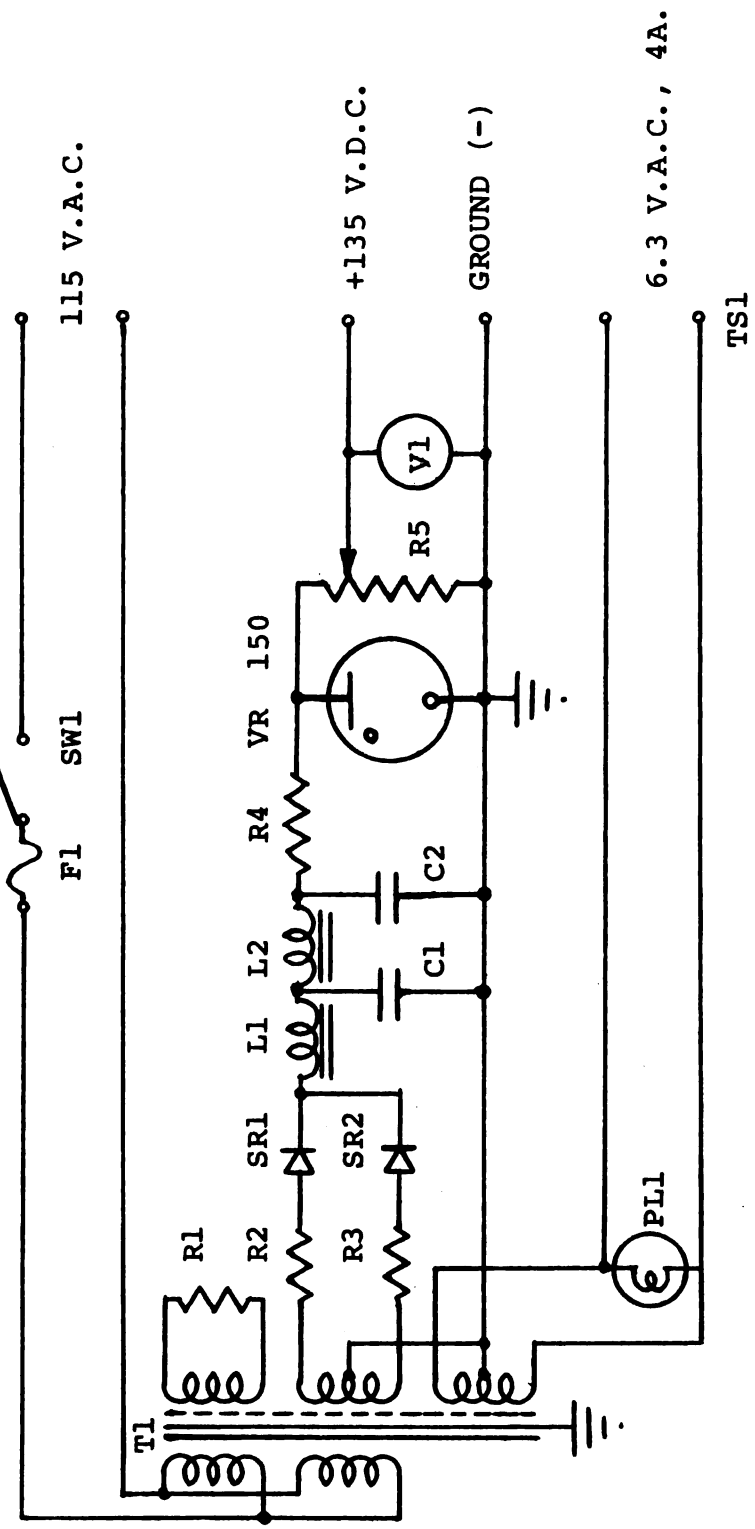

Figure A1. Schematic diagram of 135 volt power supply.